EVOLUTION OF RODINGITIC DYKES: METASOMATISM AND METAMORPHISM IN THE MOUNT AVIC SERPENTINITES (ALPINE OPHIOLITES, SOUTHERN AOSTA VALLEY)

Matteo Panseri✉, **Emanuele Fontana** and **PaolaTartarotti**

Dipartimento di Scienze della Terra, Università di Milano, Italy.
✉ *Corresponding author, e-mail: matteo.panseri@unimi.it*

Keywords: *Rodingite, metasomatism, Piemonte ophiolite. Western Alps.*

ABSTRACT

The Mount Avic ophiolite mainly consists of a large mass of serpentinites, which constitutes the base of a subunit of the Piemonte ophiolitic nappe. Serpentinites represent the mantle portion of the oceanic lithosphere of the Mesozoic Tethys and consist of antigorite-titanian clinohumite-diopside schists as products of oceanic metasomatism and tectono-metamorphic evolution of the Alpine orogeny, at the expense of abyssal peridotite mineral assemblage. The serpentinite mass includes metagabbro pods (without metasomatic alteration) and associated rodingitic dykes. Various rodingitic dykes can be distinguished on the basis of their mineralogical assemblages. The main assemblage consists of ugranditic garnet, chlorite ± diopside ± epidote ± vesuvianite. We observed also some other peculiar rodingites such as vesuvianite-chlorite-, diopside-epidote-chlorite-, and diopside-chlorite-bearing rodingites, as distinctive of the Mount Avic massif, as well as rodingitic reaction zones and foliated rodingites with chlorite, diopside, or epidote. These mineral assemblages are strictly related to the chemistry of the protolith (probably mafic dykes within serpentinite), as well as to the oceanic rodingitization during the serpentinization event and to the Alpine evolution that affected the Mount Avic massif.

INTRODUCTION

The term "rodingite" has been introduced for the first time to describe altered gabbros from the New Zealand serpentinitic massif (Bell et al., 1911) and then it has been employed for all rocks affected by Ca-metasomatism. The definition of rodingite proposed by "IUGS Subcommission on the Systematic of Metamorphic Rocks" (Zharikov et al., 2007) highlights that rodingite "is a metasomatic rock primarily composed of grossular-andradite garnet and calcic pyroxene". Other minerals as vesuvianite, epidote, scapolite, and iron ores are typical accessories.

Rodingitization usually involves mafic rocks as gabbro and basalt associated with serpentinized ultramafic rocks in the Archean - Paleoproterozoic mafic-ultramafic sequences (e.g., Anhaeusser, 1978; Schandl et al., 1989; Attoh et al., 2006), in the metamorphosed and un-metamorphosed ophiolitic complexes (e.g., Dubinska and Wiewiora, 1999; Hatzipanagiotou and Tsikouras, 2001; Hatzipanagiotou et al., 2003; Li et al., 2004; 2008), and in the present-day ocean floor (Honnorez and Kirst, 1975; Johnson, 1992; Fruh-Green et al., 1996; Kelemen et al., 2003). The chemical reactions that produce Ca-rich, SiO_2-undersatured metasomatic rocks (Coleman, 1966; 1977; Sarp and Deferne, 1978; Schandl et al., 1989) are due to fluids circulation. The source of this fluids could be related to serpentinization (Coleman, 1967; Honnorez and Kirst, 1975; Sarp and Deferne, 1978), but some studies suggest that the source of rodingitization is a Ca-rich hydrothermal fluid not related to serpentinization (e.g., De, 1972; Hall and Ahmed, 1984; Hatzipanagiotou and Tsikouras, 2001).

This paper documents the occurrence of rodingites within the Mount Avic massif, pertaining to the metaophiolite nappe system of the Italian Western Alps. Our aim is to describe in detail the mineralogical and textural features of rodingitic dykes and to discuss their metasomatic and metamorphic evolution.

GEOLOGICAL SETTING OF THE NW ALPS OPHIOLITES

The meta-ophiolites of the NW Alps (Fig. 1) are remnants of the Mesozoic Tethyan Ocean involved into subduction during the convergence between the European and African Plates, started in the Cretaceous (Bearth, 1967; Dal Piaz et al., 1972; Caby et al., 1978; Martinotti and Hunziker, 1984; Nicolas et al., 1990; Polino et al., 1990; Stampfli and Marchant, 1997). In the southern Swiss area and in the northern Aosta Valley (north of the Aosta-Ranzola fault, ARF in Fig. 1) two main Alpine ophiolite units have been defined: the Zermatt-Saas (ZS) Unit and the Combin (CO) Unit (Bearth, 1967; Dal Piaz and Ernst, 1978; Sartori and Thelin, 1987; Ballévre and Merle, 1993; Michard et al., 1996). The ZS ophiolite represents the oceanic lithosphere of the Piemontese-Ligurian basin. It consists of former mantle rocks, today represented by antigorite-Ti-clinohumite schists cut by rodingitic dykes (Bearth, 1967; Dal Piaz, 1967), metagabbroic bodies (e.g., Allalin gabbro; Chinner and Dixon, 1973), and metabasalts (basalt flows, pillow lavas and hyaloclastites) hosting sulphide-ore deposits. The ZS ophiolite is capped by a meta-sedimentary cover consisting of metacherts, some with manganiferous oxides and silicates, marble, calcschists. In the Riffelberg-Garten area (Swiss side) and in the Breuil-Ayas area (Italian side), the ZS cover includes a heterogeneous volcano-sedimentary unit consisting of volcanic turbidites (Dal Piaz, 1965; Bearth, 1967; Campari et al., 2004). The CO Unit is made of metasediments (calcschists and quarzitic schists) interbedded with slices of prasinite, metagabbro, and serpentinite. At the base of the Combin Unit, exotic sheets of continental origin occur, known as the Frilihorn series on the Swiss side (Marthaler, 1984; Sartori and Thelin, 1987), and as the Pancherot-Cime Bianche Bettaforca Unit on the Italian side (Dal Piaz, 1988).

The ZS and CO thrust Units differ for their contrasting

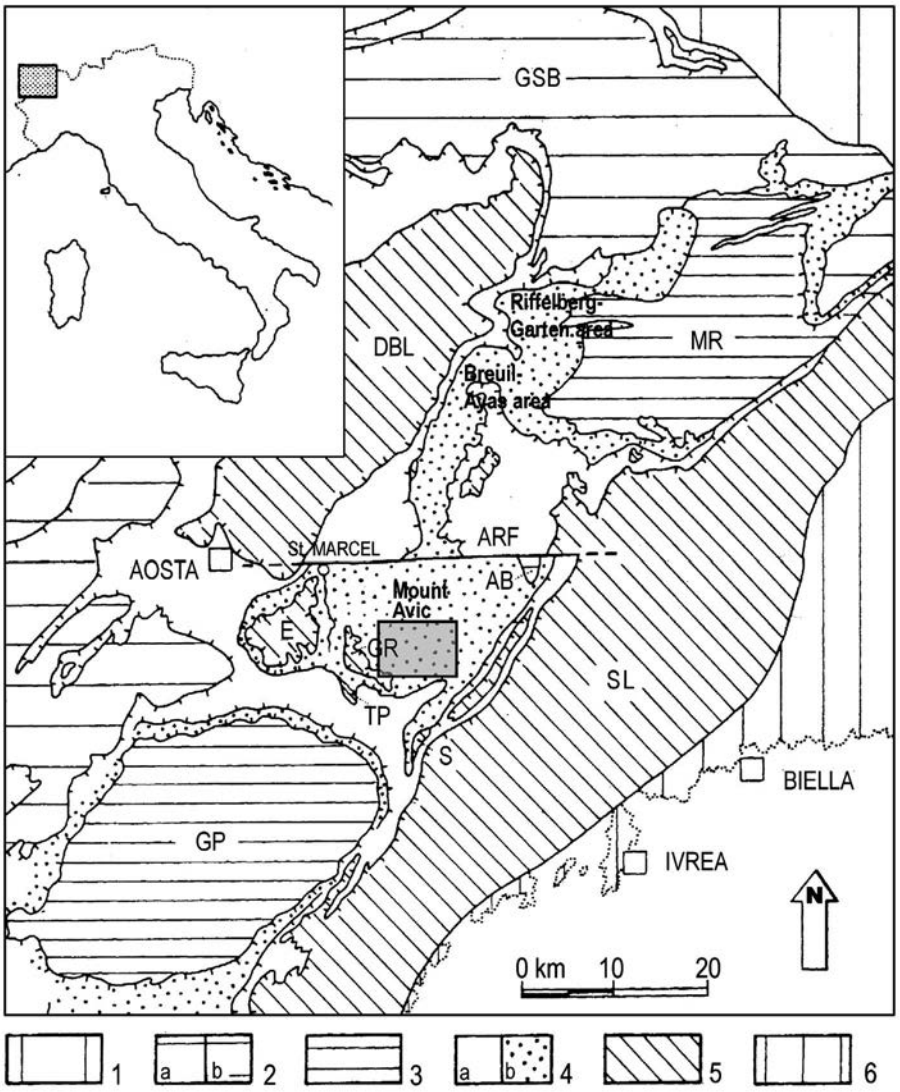

Fig. 1 - Tectonic sketch-map of the internal NW Alps showing the occurrence of metaophiolites (Baldelli et al., 1985). 1) Lower Penninic nappes and Valais calcschists zone. 2) Subbriançonnais (a) and Briançonnais (b) units. 3) Upper Penninic Monte Rosa (MR), Arcesa-Brusson (AB) and Gran Paradiso (GP) nappe system. 4) Piedmont Ophiolite nappe system: a) dominantly sedimentary units including thin sheets derived from ocean facing continental edges (Combin type); b) dominantly ophiolitic units with eclogitic metamorphism (Zermatt-Saas type). 5) Austroalpine Sesia-Lanzo (SL) and Dent Blanche (DBL) nappe system, including Mt. Emilius (E), Glacier Rafray (GR), Tour Ponton (TP) and Santanel (S) southern Klippen. 6) Southern Alps. ARF: Aosta-Ranzola fault. Grey box represents the study area (Mount Avic serpentinitic massif).

metamorphic evolution during the Alpine orogeny. The ZS is characterized by LT-HP to UHP mineral assemblages of early Alpine age (e.g. garnet, omphacite, rutile, zoisite in Fe-Ti-metagabbros and metamorphosed basalts; coesite in metaquartzites). These assemblages attest a fossil subduction zone (Dal Piaz et al., 1972; Ernst and Dal Piaz, 1978; Oberhaensli, 1980; Reinecke, 1991; Van der Klauw et al., 1997). They were later overprinted, during a polyphase decompressional evolution, by blueschist (glaucophane, chloritoid, white mica) to greenschist (actinolite, albite, chlorite, epidote) facies assemblages (Bearth, 1967; Dal Piaz and Ernst, 1978; Barnicoat and Fry, 1986). Recent estimations of the P-T conditions in the ZS Unit (Pfulwe eclogites and glaucophanites) suggest a peak eclogite-facies metamorphism at 2.7-2.8 GPa and 580°C (Bucher et al., 2005). Glaucophane-bearing metabasalts, interpreted as being hydrated during ocean-floor metamorphism, may be coeval with eclogites deriving from unaltered basalts (Oberhaensli, 1982; Martin and Tartarotti, 1989; Bowtell, 1991). The CO Unit mostly displays greenschist facies mineral associations (actinolite, albite, chlorite, epidote), although rare blueschist facies minerals (e.g., sodic amphibole) have been found (Cortiana et al., 1999; Desmons et al., 1999).

In the southern Aosta Valley (NW Italian Alps), south of the ARF (Fig. 1), metaophiolites belong to the Piemonte ophiolitic nappe. Due to their lithological association and metamorphic imprint, these ophiolites are similar to the ZS Unit comprising antigorite-Ti-clinohumite-bearing serpentinites, minor Fe-Ti- and Mg-metagabbros, metabasalts, and meta-sedimentary rocks that experienced early Alpine metamorphism under eclogite-blueschists facies conditions (Baldelli et al., 1985; Castelli, 1985; Ballévre et al., 1986; Martin and Kienast, 1987; Benciolini et al., 1988; Martin and Tartarotti, 1989; Novo et al., 1989; Tartarotti and Caucia, 1993). The Mesozoic sequence is overthrust by the pre-Triassic Austroalpine Mt. Emilius, Glacier-Rafray and Tour Ponton *klippen* (Fig. 1). The oceanic crustal units are well exposed in the Clavalité - St. Marcel area (Fig. 1), where they are mainly represented by eclogitic Fe-Ti- and Mg-metagabbros, gabbro-derived metarkose, garnet-lawsonite (pseudomorphed)-bearing glaucophanites including eclogitic boudins, garnet-chloritoid chloriteschists, minor talcschists (Nervo and Polino, 1977; Krutow-Mozgawa, 1988; Tartarotti, 1988; Martin and Tartarotti, 1989; Martin et al., 2008). The meta-sedimentary cover mainly consists, from bottom to top, of deep sea Mn-Fe-rich metacherts, marble and calcschists which are equivalent to the Upper Jurassic-Lower Cretaceous sediments of the Ligurian Apennines (Tartarotti et al., 1986). The mantle section is represented by widespread serpentinite sheets and by a huge serpentinite massif cropping out in the Mount Avic area (Figs. 1 and 2). Estimations of the peak P-T conditions in the St.

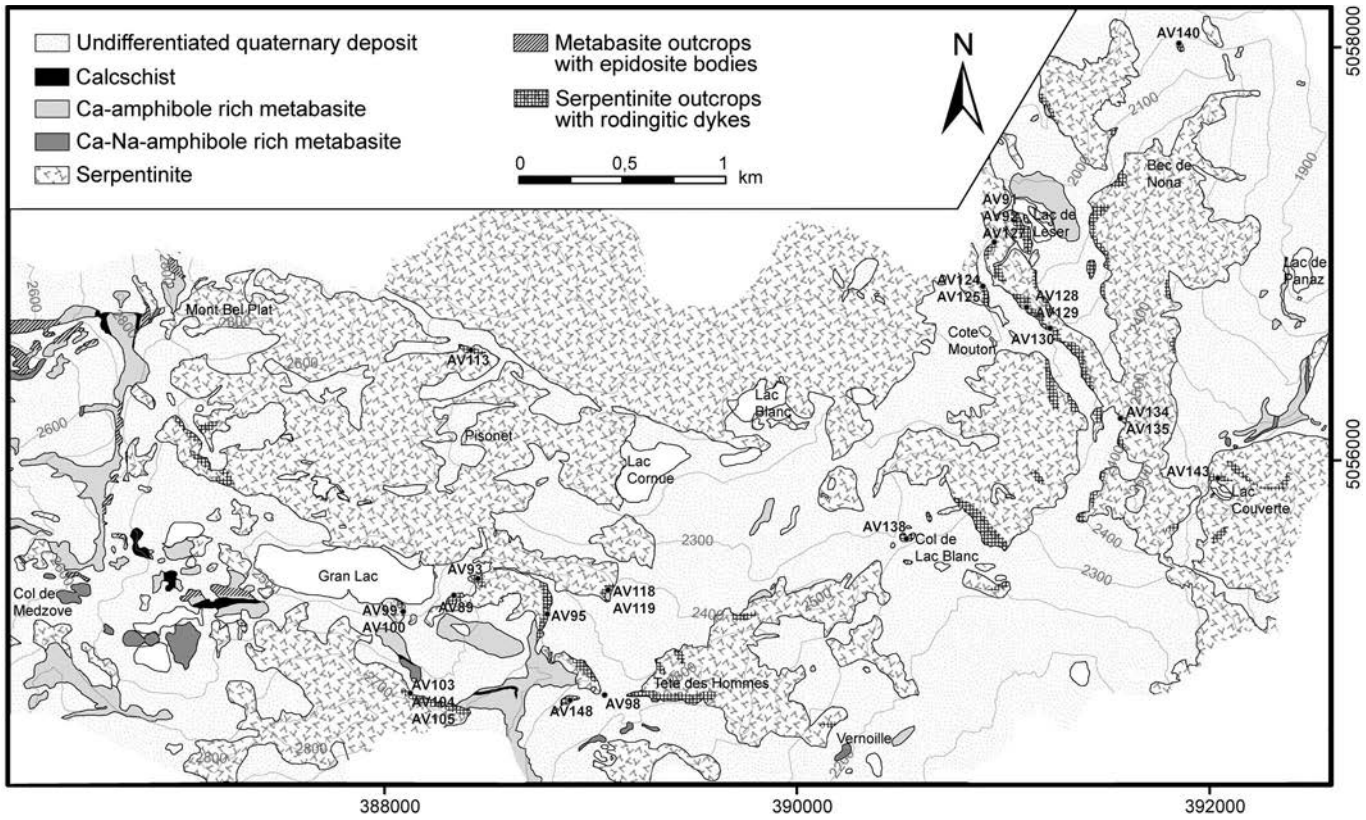

Fig. 2 - Lithological map of the studied area in the Mount Avic serpentinite massif as obtained by original field mapping. Location of rodingitic dyke samples is reported. UTM coordinate system: Datum ED 1950; Zone 32N.

Marcel Valley ophiolites have been recently performed by Martin et al. (2008), yelding temperature values of 550 ± 60°C and pressure values of 2.1 ± 0.3 GPa, that are higher than those previously calculated in the same area by other authors.

FIELD RELATIONS

The Mount Avic is a huge massif of serpentinized mantle peridotite (Figs. 1 and 2) that crops out as a tectonic window south of the ARF, in the eastern part of the EW-trending Aosta Valley (Tartarotti and Martin, 1991; Diella et al., 1994; Fontana et al., this volume). The exposed serpentinite area is about 180 km^2 wide. In this paper we deal with the southern area of the Mount Avic serpentinite massif. Serpentinites contain metamorphosed mafic bodies and rodingites, with minor chloriteschist and talcschist lenses. Metamorphosed mafic rocks occur either as tectonized pods, surrounded by serpentinites, or as tectonic sheets. The latter consist of mafic rocks with rodingitic reaction zones, often associated with calcschists slices, and sulphide-rich epidosites. All these rock types build up a few hundreds meters- thick crustal unit overthrusting the Mount Avic serpentinitic Unit (Fig. 3).

Serpentinites

Serpentinites occur as weakly to strongly deformed (mylonitic) rocks. Weakly deformed serpentinites are the most abundant rock type. Their weathered surface is ochre- to reddish-brown-coloured, whilst on the fresh surface these rocks are dark green to black. Mylonitic serpentinites are fine-grained and foliated, and frequently occur near the contact with other rock types, but mylonitic bands were also found within low-deformed serpentinites. Serpentine is finally observed as lineated acicular crystals or fibres (cm-sized) restricted to dm-sized bands.

The serpentinite mainly consists of serpentine (0.1-1 mm-sized antigorite crystals; > 90 vol.%) and magnetite (up to mm-sized, 5-10 vol.%, Fontana et al., this volume), defining the main foliation. Magnetite often occurs as mineral aggregates that mark the mineral lineation. Less serpentinized rocks consist of olivine (Fo_{90-95}), clinopyroxene (diopside), Ti-clinohumite, antigorite, tremolite, and late calcite. Olivine, diopside, and Ti-clinohumite occur as mm-sized porphyroblasts, often preserving relict mantle textures (see Fontana et al., this volume). Porphyroblasts are more or less recrystallized into finer-grained neoblasts. Pseudomorphs of antigorite replacing mm-sized former minerals may also represent relics of the original mantle texture. Olivine, diopside, and Ti-clinohumite porphyroblasts frequently occur filling boudinaged ribbons wrapped by the antigorite foliation. In the eastern part of the study area, serpentinite is the host rock of rodingitic dykes and mafic rocks.

Metamorphosed mafic rocks (metabasite)

Metamorphosed mafic rocks mainly occur in the western side of the study area (Fig. 2), within the crustal unit overthrust on the serpentinite massif. We also observed m- to 100 m-sized mafic pods within the serpentinites. The contact between these pods and the host serpentinite is not rodingitized. Metamorphosed mafic rocks from the pods and those from the western crustal unit show similar features. We distinguished two main mafic rocks:

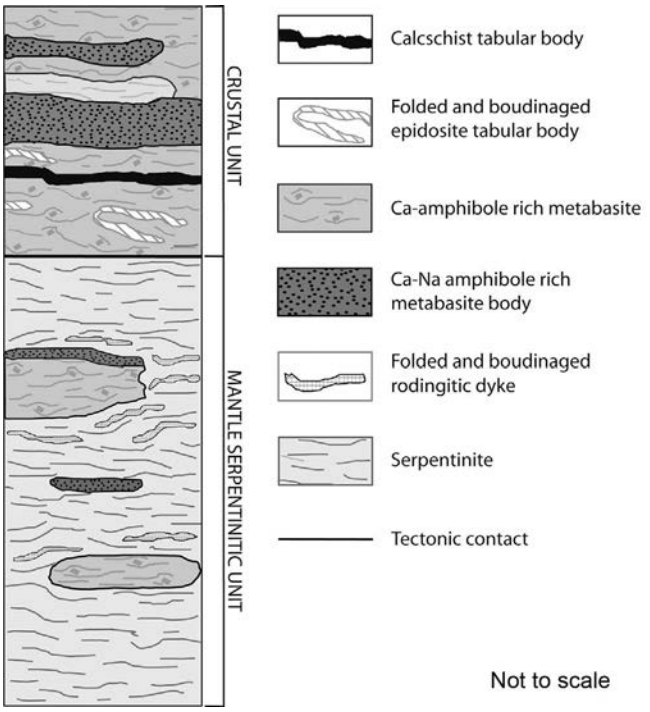

Fig. 3 - Simplified litho-stratigraphic section of the Mount Avic ophiolite. Calcschist and serpentinite in the Crustal Unit are tectonically interlayered.

– Ca-amphibole-rich rocks (similar to the Mg-(Cr)-metagabbro cropping out in the ZS Unit and Clavalité-St. Marcel area; Martin and Tartarotti, 1989);
– Ca-Na-amphibole-rich rocks (similar to the Fe-Ti-metagabbro and metabasalts cropping out in the ZS Unit and Clavalité - St. Marcel area; Martin and Tartarotti, 1989).

Transition from Ca-amphibole-rich rocks to Ca-Na-amphibole-rich rocks with eclogitic relics is always gradual.

Ca-amphibole-rich metabasite consists of albite (40-50 vol.%), clinozoisite (up to 30 vol.%), amphibole (20-30 vol.%, Mg-hornblende and tremolite-actinolite), ± zoisite, ± Cr-amphibole (smaragdite), ± chlorite, ± quartz, ± white mica and fuchsite (Panseri, 2003; Fontana, 2005). The coarse-grained flaser-textured portions show mm-sized clinozoisite aggregates and mm- to cm-sized poikilitic albite including mm-sized amphibole (Mg-hornblende and tremolite-actinolite). Mg-hornblende, tremolite-actinolite, chlorite (0.1-1 mm) and mm-cm-sized fuchsite form discontinuous cleavage domains. These domains surround albite-clinozoisite eyes and mark a slight, wavy foliation. The fine-grained rock portions (0.1-1 mm-size) show the same mineralogical association, but they show a pervasive and continuous foliation, marked by Ca-amphibole + fuchsite cleavage domains and albite + clinozoisite lithons. Ca-amphibole-rich metabasites are completely retrogressed to greenschist facies and do not show magmatic or HP mineral relics.

Ca-Na-amphibole-rich metabasites occur in small outcrops associated with Ca-amphibole-rich metabasite; they consist of eclogitic relics (omphacite up to 30 vol.% and Alm-Py-rich garnet ~ 20 vol.%), and of Na- and Ca-Na-amphibole (20-30 vol.%, glaucophane, barroisite-winchite, richterite-katophorite), albite (10-20 vol.%), clinozoisite and zoisite (~ 10 vol.%), ± rutile, ± green biotite. The HP assemblage (garnet, omphacite and glaucophane) is partly retrogressed: fine-grained Ca-Na-amphibole replaces Na-amphibole at the rim (mm-cm-sized glaucophane); omphacite (mm to cm in size) is partially uralitized; chlorite and green biotite (up to 0.1 mm in size) overgrow garnet crystals. Fine-grained albite and Ca-amphibole (actinolite) form the low-P assemblage (greenschist facies). Metabasite samples commonly show a slight foliation marked by amphibole, but coarse-grained rocks characterized by a granoblastic texture were also observed.

Epidosites

The western crustal unit contains reddish tabular epidosite bodies, up to 2m thick and 100m long. Epidosite consists mainly of epidote, albite, ± diopside, ± quartz, ± Ca-(Na)-amphibole, ± chlorite, ± white mica, ± titanite, ± sulphide, ± magnetite (Buscemi, 2003). Boudinage and multi-stage folding affected these epidosite bodies.

Metasedimentary rocks

Metasedimentary rocks (mostly calcschists) crop out near Gran Lac and Mont Bel Plat (Fig. 2). They form a 1- to 10 m thick tabular body interbedded with metabasite of the crustal unit. Calcschist consists of white mica, plagioclase, garnet, white-grey epidote, and calcite.

Rodingites

Rodingitic dykes are enclosed in serpentinites, especially in the southern and eastern sides of the study area. We often found a concentration of rodingitic dykes around metabasite pods (Figs. 2 and 4). This finding suggests a genetic relation between this latter rock and rodingites. The dykes, up to 2m- thick and several meters long, are always parallel to the serpentinite foliation and are surrounded by mm- cm-sized chlorite-rich layer, formally named blackwall. They are often deformed by boudinage or by a multi-stage folding. Rodingites are slightly deformed or show a weak foliation marked by chlorite and a mineralogical layering (garnet or vesuvianite or pyroxene layers interbedded with chlorite). By contrast, we locally observed strongly foliated rodingites. These latter crop out around some rodingitic dykes and are always surrounded by chlorite-rich blackwalls.

Rodingites consist of Ca-rich mineral assemblages: Ca-garnet, epidote, diopside, vesuvianite and calcite. Chlorite is present within the dykes and is the main mineral forming the blackwalls surrounding all the rodingitic dykes. The mineral assemblage is quite variable. At the outcrop scale, the following rodingite types were distinguished:

1- garnet-rodingitic dykes (Fig. 5a, largely cropping out around metabasite pods near Gran Lac and Lac de Leser): pink-reddish-brown rodingitic dykes consisting of garnet, chlorite, ± pyroxene, ± vesuvianite;

2- vesuvianite-rodingitic dykes (Fig. 5b, near Cote Mouton, Tete des Hommes and Bec de Nona): yellow rodingite consisting of vesuvianite, chlorite, ± garnet;

3- foliated rodingites with diopside and chlorite, centimetric to decimetric in size, cropping out at the contact between garnet rodingitic dykes and serpentinite and bordered by a chloritic blackwall (Fig. 5c, near Cote Mouton and near Gran Lac); foliated rodingites with chlorite, green and white epidote, ± pyroxene (east of Gran Lac) enclosing thin rodingitic dykes (cm in size and consisting of garnet and chlorite);

4- rodingitic reaction zones at the contact between metabasite pods and serpentinites (south of Lac Cornue).

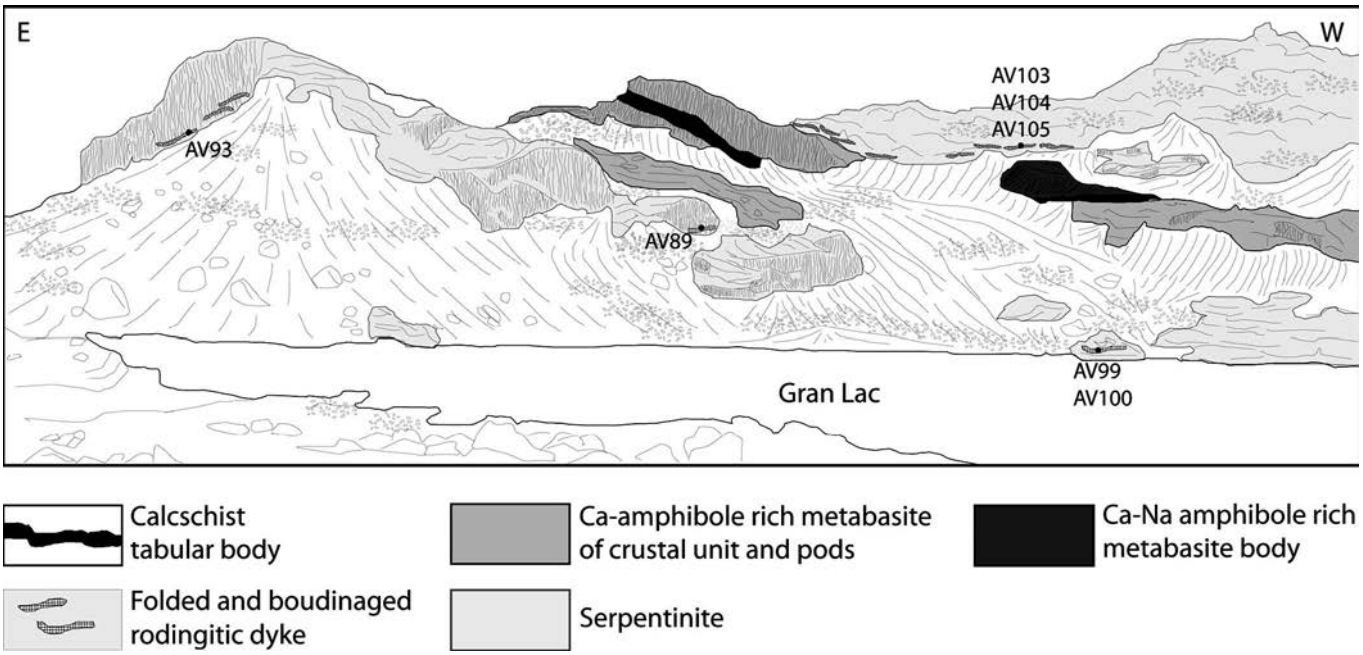

Fig. 4 - Panoramic drawing of the Gran Lac area. Rodingitic dykes crop out around metagabbro bodies.

They consist of m- 20m-thick tabular bodies characterized by garnet, green epidote, chlorite and calcite veins. Mineralogical layering, marked by alternating garnet and epidote levels (Fig. 5d), is parallel to the edge of the reaction zones.

We also mapped (near Cote Mouton and Tete des Hommes; see Fig. 2) and analyzed some mixed garnet/vesuvianite rodingitic dykes, usually characterized by garnet-chlorite core and vesuvianite-chlorite rim (Fig. 5e). The transition from garnet to vesuvianite zones is gradual.

Finally we observed pyroxene-rich dykes surrounded by a mm- sized chlorite-rich blackwall, namely:

– pyroxene-epidote dykes: white-grey dykes with pyroxene, epidote (clinozoisite or zoisite) and chlorite, cropping out near Cote Mouton (see Fig. 2);
– pyroxene dykes (Fig. 5f): white rocks cropping out north of Pisonet and near Col de Lac Blanc. They consist of diopside, minor chlorite, and locally show reddish alteration coating (Col de Lac Bland dyke, see Fig. 2).

Pyroxene-rich-dykes cannot be considered as rodingites s.s. because of the lack of garnet or vesuvianite.

PETROGRAPHY AND MINERAL COMPOSITION OF THE MOUNT AVIC RODINGITES

In order to understand the structure and evolution of the Mount Avic ophiolitic complex and metasomatic events, we performed thin section studies on rodingite samples. We also carried out EDS analyses to characterize the rodingite mineral assemblages. Mineral chemistry data and backscattered images were collected by scanning electron microscope (SEM) Cambridge System Stereoscan 360, equipped with Energy Dispersive X-ray Spectroscopy (EDS Link ISIS), at the Consiglio Nazionale delle Ricerche (CNR)-Department of Earth Sciences (Milano University). The correction program used is ZAF4 (Pouchou and Pichoir, 1985). Operating conditions were as follows: accelerating voltage = 20 kV; working distance = 25 mm; probe beam = 400 pA; count time = 50 s. Selected analyses representing the mineral composition of rodingite samples are summarized in Tables 1 and 2. We also performed XRD analyses with a PANalytical X'Pert Pro MPD powder diffractometer, equipped with an X'Celerator multichannel detector, with CuKalpha wavelength (1.5418 Å). The data collections were from 5 to 90° 2ϑ, with a step size of about 0.02° and a counting time of 25 seconds per step.

Rodingite types that were distinguished in the field also show distinct mineral assemblages and mineral composition. A chloritic blackwall surrounds all rodingite dykes and mainly consists of chlorite (90-95 vol.%), with minor magnetite. It also shows low concentrations of garnet, diopside, or vesuvianite. Chloritic blackwalls often show gradual transition to rodingite and to serpentinite.

Garnet-rodingitic dykes

Garnet-rodingitic dykes mainly consist of garnet (up to 80 vol.%) and chlorite (20-50 vol.%, Fig. 6a), with variable amounts of diopside (0-30 vol.%), spinel group minerals (mostly magnetite) or more rarely titanite, epidote, clinozoisite and ilmenite. Grain size ranges from mm- to cm-. Granoblastic texture is the most common, although a strong foliation marked by chlorite and garnet layers may be occasionally present. Locally, we observed diopside with mechanical twinning, surrounded by chlorite foliation. Transition from the rodingite dyke to its blackwall is gradual and characterized by an increasing amount of chlorite and by a penetrative foliation. The blackwall consists of chlorite (90-95 vol.%, up to mm in size) ± garnet, ± magnetite.

Garnet is mainly grossular (up to 95%). XRD analyses evidence the lack of hydrogrossular and other hydrogarnet. Locally Cr-rich-garnet (46% uvarovite, 47% grossular; sample AV91, Fig. 6b) grows at the rim of chromite or chromite-hercynite series mineral (see sample AV128, Table 3). We also observed Ca-Fe-rich-garnet (58-63% grossular, 24-30% almandine, 4-11% andradite) in samples AV103 and AV105 (Ca-Fe-garnet-rodingitic dykes from

Table 1 - Representative EDS analyses of rodingite minerals: chlorite and garnet.

	Chlorite							
Analises	**99-166**	**128-76**	**105-28**	**130-118**	**124-314**	**113-188**	**100-64**	**119-28**
	Grs rod	Grs rod	Fe-Gr rod	Ves rod	Px-Ep	Px dik	Fol rod	Rod RZ
SiO_2	30,1	29,4	26,9	31,1	29,0	34,2	33,8	27,5
Al_2O_3	18,6	22,2	18,7	20,1	18,7	12,1	13,1	19,2
FeO tot.	4,7	2,6	22,3	2,4	7,0	3,2	4,5	22,5
MgO	29,5	31,8	17,1	32,1	28,1	33,8	33,6	17,7
CaO	0,0	0,0	0,1	0,0	0,0	0,1	0,1	0,1
Na_2O	0,0	1,2	0,0	1,2	1,0	0,0	0,0	1,2
K_2O	0,1	0,0	0,0	0,1	0,1	0,0	0,0	0,0
TiO_2	0,0	0,0	0,1	0,2	0,0	0,2	0,0	0,0
MnO	0,0	0,0	0,2	0,1	0,0	0,1	0,0	0,9
Cr_2O_3	0,4	0,0	0,1	0,0	0,0	1,1	0,2	0,0
NiO	0,2	0,0	0,0	0,0	0,0	0,1	0,4	0,0
Total	83,6	87,2	85,4	87,1	83,9	84,9	85,7	88,9
Ions on the basis of 28O								
Si	6,0	5,5	5,7	5,8	5,8	6,6	6,5	5,7
Al IV	2,1	2,5	2,3	2,2	2,2	1,4	1,5	2,3
Total	8,0	8,0	8,0	8,0	8,0	8,0	8,0	8,0
Al VI	2,3	2,5	2,4	2,3	2,2	1,4	1,5	2,3
Fe^{2+} tot.	0,8	0,4	4,0	0,4	1,2	0,5	0,7	3,9
Mg	8,7	8,9	5,4	9,0	8,4	9,8	9,7	5,4
Ca	0,0	0,0	0,0	0,0	0,0	0,0	0,0	0,0
Na	0,0	0,4	0,0	0,4	0,4	0,0	0,0	0,5
K	0,0	0,0	0,0	0,0	0,0	0,0	0,0	0,0
Ti	0,0	0,0	0,0	0,0	0,0	0,0	0,0	0,0
Mn	0,0	0,0	0,0	0,0	0,0	0,0	0,0	0,2
Cr	0,1	0,0	0,0	0,0	0,0	0,2	0,0	0,0
Ni	0,0	0,0	0,0	0,0	0,0	0,0	0,1	0,0
Total	11,9	12,2	11,9	12,1	12,2	11,9	12,0	12,3

Grs rod	Grossular rodingite
Fe-Gr rod	Ca-Fe-garnet rodingite
Ves rod	Vesuvianite rodingite
Fol rod	Foliated rodingite
Rod RZ	Rodingitic reaction zone
Px-Ep	Pyroxene-epidote dyke
Px	Pyroxene dyke

	Garnet								
Analises	**91-43**	**92-89**	**99-153**	**103-298**	**105-01**	**129-109**	**129-112**	**134-119**	**119-32**
	Grs rod	Grs rod	Grs rod	Fe-Gr rod	Fe-Gr rod	Ves rod	Ves rod	Ves rod	Rod RZ
SiO_2	39,5	35,7	37,5	37,4	37,7	37,0	37,3	36,0	38,5
Al_2O_3	21,9	5,1	14,6	20,6	18,6	11,0	21,9	4,1	19,2
ZrO_2	0,0	0,0	0,0	0,0	0,0	0,0	0,0	0,0	0,0
TiO_2	0,0	0,7	2,2	0,4	0,2	0,1	0,2	0,7	0,2
Cr_2O_3	0,0	13,4	1,7	0,0	0,0	3,6	0,1	0,1	0,0
Fe_2O_3	0,8	10,1	7,4	2,1	5,1	12,3	2,3	24,8	4,2
FeO	1,4	0,0	0,0	14,6	10,9	0,0	0,0	0,0	11,9
MnO	0,2	0,2	0,0	0,2	0,6	0,5	0,0	0,3	0,6
MgO	0,3	0,1	0,2	0,8	0,7	0,1	2,7	0,1	0,6
CaO	35,3	33,7	35,8	22,7	25,2	35,0	35,7	33,7	25,1
Na_2O	0,1	0,1	0,1	0,6	0,7	0,1	0,1	0,0	0,4
Total	99,4	99,2	99,3	99,4	99,7	99,6	100,1	99,8	100,8
Ions of the basis of 12 O									
Si	3,0	2,9	2,9	2,9	3,0	3,0	2,8	3,0	3,0
Al (IV)	0,0	0,1	0,1	0,1	0,0	0,0	0,2	0,0	0,0
Site Z	3,0	3,0	3,0	3,0	3,0	3,0	3,0	3,0	3,0
Al (VI)	2,0	0,4	1,3	1,9	1,7	1,0	1,8	0,4	1,7
Zr	0,0	0,0	0,0	0,0	0,0	0,0	0,0	0,0	0,0
Ti	0,0	0,0	0,1	0,0	0,0	0,0	0,0	0,0	0,0
Cr	0,0	0,9	0,1	0,0	0,0	0,2	0,0	0,0	0,0
Fe^{3+}	0,0	0,6	0,4	0,1	0,3	0,7	0,1	1,5	0,2
Site Y	2,0	2,0	2,0	2,0	2,0	2,0	1,9	2,0	2,0
Fe^{2+}	0,1	0,0	0,0	1,0	0,7	0,0	0,0	0,0	0,8
Mn	0,0	0,0	0,0	0,0	0,0	0,0	0,0	0,0	0,0
Mg	0,0	0,0	0,0	0,1	0,1	0,0	0,3	0,0	0,1
Ca	2,9	3,0	3,0	1,9	2,1	3,0	2,9	3,0	2,1
Na	0,0	0,0	0,0	0,1	0,1	0,0	0,0	0,0	0,1
Site X	3,0	3,0	3,0	3,1	3,1	3,1	3,2	3,0	3,0
Prp	0,9	0,0	0,0	3,0	2,6	0,0	0,0	0,0	2,2
Alm	2,9	0,0	0,0	32,4	24,3	0,0	0,0	0,0	26,0
Grs	93,6	22,1	68,4	56,8	55,9	50,5	92,4	19,4	57,4
Sps	0,3	0,2	0,0	0,2	1,4	0,0	0,0	0,0	1,4
Uvt	0,0	44,0	5,4	0,0	0,0	11,7	0,3	0,4	0,0
Adr	2,3	31,5	23,1	6,3	15,2	37,5	6,8	79,3	12,3

Chlorite classification on the basis of Hey (1954).

Table 2 - Representative EDS analyses of rodingite minerals: epidote, vesuvianite, and pyroxene.

Epidote				
Analises	**99-136**	**130-105**	**124-312**	**119-7**
	Grs rod	Ves rod	Px-Ep	Rod RZ
SiO_2	39,7	39,7	38,6	38,8
TiO_2	0,1	0,2	0,0	0,1
Al_2O_3	29,0	30,6	31,8	23,8
Cr_2O_3	0,0	0,0	0,0	0,0
Fe_2O_3	6,3	4,9	2,0	13,1
FeO	0,0	0,0	0,0	0,0
MnO	0,1	0,1	0,1	0,2
MgO	0,0	0,2	0,2	0,2
CaO	24,6	24,8	24,3	23,8
Total	99,8	100,5	97,1	100,0
Ions of the basis of 25 O				
Si	6,0	6,0	5,9	6,0
Al (IV)	0,0	0,0	0,1	0,0
Total	6,0	6,0	6,0	6,0
Al (VI)	5,2	5,4	5,7	4,4
Ti	0,0	0,0	0,0	0,0
Cr	0,0	0,0	0,0	0,0
Fe^{3+}	0,7	0,6	0,2	1,5
Total	5,9	6,0	6,0	5,9
Fe^{2+}	0,0	0,0	0,0	0,0
Mn	0,0	0,0	0,0	0,0
Mg	0,0	0,0	0,0	0,1
Ca	4,0	4,0	4,0	4,0
Total	4,0	4,1	4,1	4,0

Grs rod	Grossular rodingite
Fe-Gr rod	Ca-Fe-garnet rodingite
Ves rod	Vesuvianite rodingite
Fol rod	Foliated rodingite
Rod RZ	Rodingitic reaction zone
Px-Ep	Pyroxene-epidote dyke
Px	Pyroxene dyke

Vesuvianite				
Analises	**134-107**	**129-111**	**130-109**	**140-70**
	Ves rod	Ves rod	Ves rod	Ves rod
SiO_2	36,9	36,7	38,2	38,2
Al_2O_3	18,1	18,0	17,7	15,2
MgO	2,5	2,5	2,7	2,7
FeO tot.	1,7	2,1	3,0	5,4
Cr_2O_3	0,1	0,3	0,0	0,0
TiO_2	0,2	0,1	0,1	0,2
MnO	0,1	0,0	0,0	0,1
NiO	0,0	0,0	0,0	0,0
CaO	37,0	37,0	36,2	38,4
Na_2O	0,0	0,0	0,5	0,0
K_2O	0,1	0,0	0,0	0,0
Total	94,8	94,7	95,5	94,8
Ions of the basis of 50 total cations				
Si	17,8	17,6	18,0	17,9
Al (IV)	0,2	0,4	0,0	0,1
Site (IV)	18,0	18,0	18,0	18,0
Al (VI)	4,0	4,0	4,0	4,0
Site A	4,0	4,0	4,0	4,0
Al (VI)	5,8	5,8	5,8	4,3
Mg	1,8	1,8	1,9	1,9
Fe^{3+}	0,0	0,0	0,0	1,4
Cr	0,0	0,1	0,0	0,0
Ti	0,3	0,3	0,3	0,3
Mn	0,0	0,0	0,0	0,1
Ni	0,0	0,0	0,0	0,0
Site G	8,0	8,0	8,0	8,0
Fe^{2+}+Fe^{3+}	0,7	0,9	1,2	0,7
Al (VI)	0,2	0,1	0,1	0,0
Site B	0,9	0,9	1,2	0,7
Ca	19,1	19,0	18,3	19,3
Na	0,0	0,0	0,4	0,0
K	0,0	0,0	0,0	0,0
Site Ca	19,1	19,1	18,8	19,3
X_{Mg} (Fe^{tot})	0,7	0,7	0,6	0,5

Pyroxene								
Analises	**99-142**	**100-67**	**103-287**	**103-290**	**113-182**	**119-24**	**124-313**	**134-115**
	Grs rod	Fol rod	Fe-Gr rod	Fe-Gr rod	Px	Rod RZ	Px-Ep	Ves rod
SiO2	53,3	55,0	53,2	52,44	55,7	53,8	54,2	55,3
Al_2O_3	1,9	0,3	1,4	3,07	0,1	0,9	2,0	0,0
Fe_2O_3	1,0	0,0	6,7	8,83	0,0	5,2	3,4	0,0
FeO	1,7	2,2	2,1	1,33	1,6	1,1	0,0	0,6
MgO	16,0	16,5	12,6	10,39	17,8	14,1	15,1	17,8
MnO	0,3	0,2	0,0	0,00	0,0	0,1	0,2	0,1
TiO_2	0,4	0,0	0,0	0,07	0,2	0,0	0,0	0,1
Cr_2O_3	0,2	0,1	0,0	0,00	0,1	0,0	0,0	0,0
CaO	24,7	25,6	22,0	18,56	25,3	23,7	22,6	25,9
Na_2O	0,4	0,0	2,4	4,13	0,0	1,7	2,2	0,0
Total	99,9	100,0	100,3	98,82	100,7	100,6	99,5	99,7
Ions of the basis of 6 O								
Si	1,9	2,0	2,0	1,96	2,0	2,0	2,0	2,0
Al (IV)	0,1	0,0	0,0	0,04	0,0	0,0	0,0	0,0
Sito (IV)	2,0	2,0	2,0	2,00	2,0	2,0	2,0	2,0
Al (VI)	0,0	0,0	0,0	0,09	0,0	0,0	0,1	0,0
Fe^{3+}	0,0	0,0	0,2	0,25	0,0	0,1	0,1	0,0
Fe^{2+}	0,1	0,1	0,1	0,04	0,0	0,0	0,0	0,0
Mg	0,9	0,9	0,7	0,58	1,0	0,8	0,8	1,0
Mn	0,0	0,0	0,0	0,00	0,0	0,0	0,0	0,0
Ti	0,0	0,0	0,0	0,00	0,0	0,0	0,0	0,0
Cr	0,0	0,0	0,0	0,00	0,0	0,0	0,0	0,0
Sito (VI)	1,0	1,0	1,0	0,96	1,0	1,0	1,0	1,0
Ca	1,0	1,0	0,9	0,74	1,0	0,9	0,9	1,0
Na	0,0	0,0	0,2	0,30	0,0	0,1	0,2	0,0
Site M2	1,0	1,0	1,0	1,04	1,0	1,0	1,0	1,0
QUAD	92,9	98,4	79,3	65,95	98,6	85,2	84,7	99,8
Wo	51,2	50,8	53,4	54,49	49,3	53,6	51,8	50,7
En	46,0	45,7	42,5	42,46	48,3	44,5	48,2	48,5
Fs	2,8	3,5	4,1	3,05	2,4	2,0	0,0	0,9
Jd	0,0	0,0	2,1	9,14	0,0	0,5	6,0	0,0
Aeg	0,0	0,0	18,6	24,91	0,0	14,3	9,3	0,0
X_{Mg} (Fe^{tot})	0,9	0,9	0,7	0,67	1,0	0,8	0,9	1,0

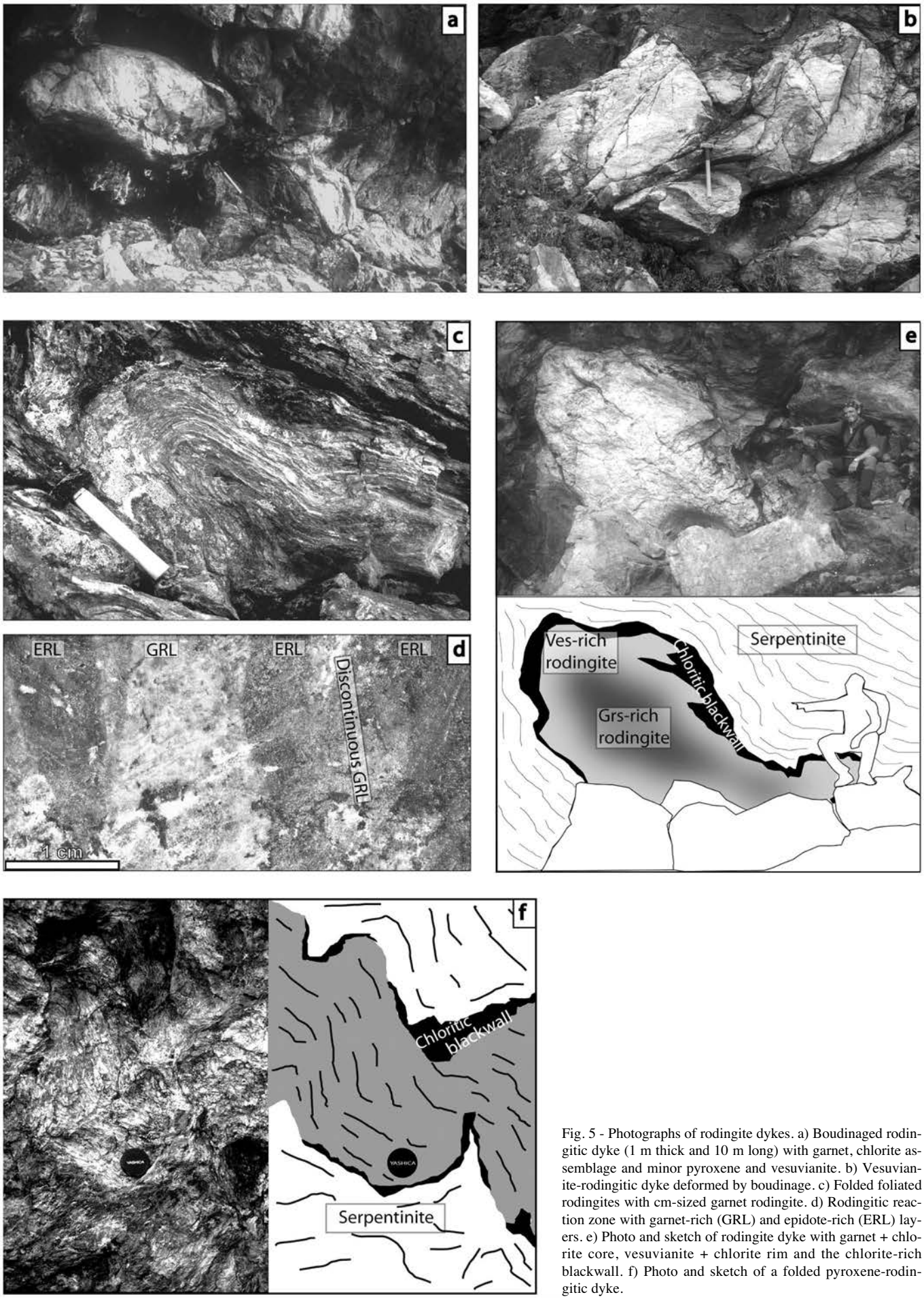

Fig. 5 - Photographs of rodingite dykes. a) Boudinaged rodingitic dyke (1 m thick and 10 m long) with garnet, chlorite assemblage and minor pyroxene and vesuvianite. b) Vesuvianite-rodingitic dyke deformed by boudinage. c) Folded foliated rodingites with cm-sized garnet rodingite. d) Rodingitic reaction zone with garnet-rich (GRL) and epidote-rich (ERL) layers. e) Photo and sketch of rodingite dyke with garnet + chlorite core, vesuvianite + chlorite rim and the chlorite-rich blackwall. f) Photo and sketch of a folded pyroxene-rodingitic dyke.

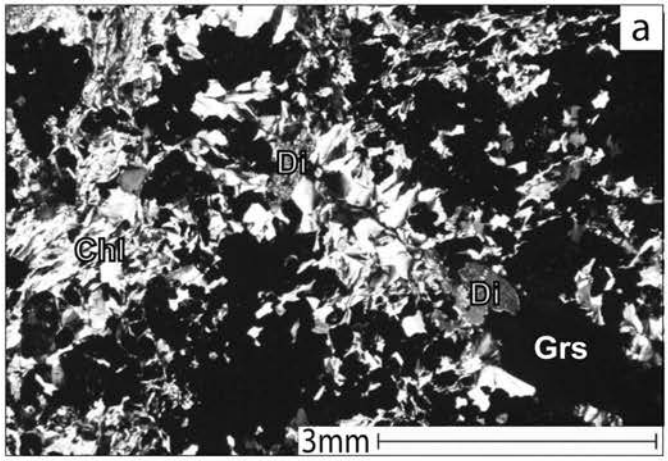

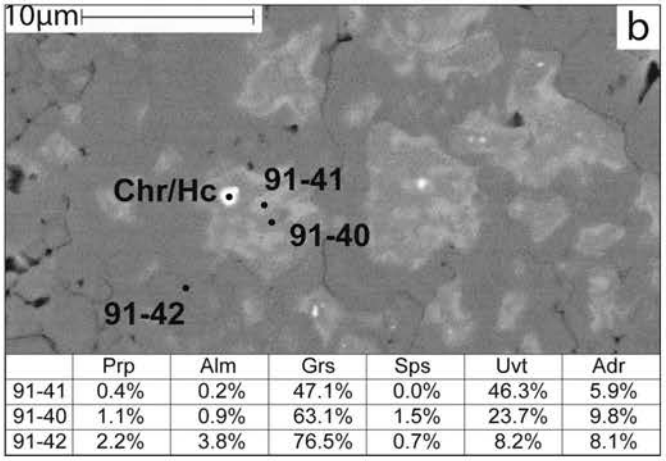

	Prp	Alm	Grs	Sps	Uvt	Adr
91-41	0.4%	0.2%	47.1%	0.0%	46.3%	5.9%
91-40	1.1%	0.9%	63.1%	1.5%	23.7%	9.8%
91-42	2.2%	3.8%	76.5%	0.7%	8.2%	8.1%

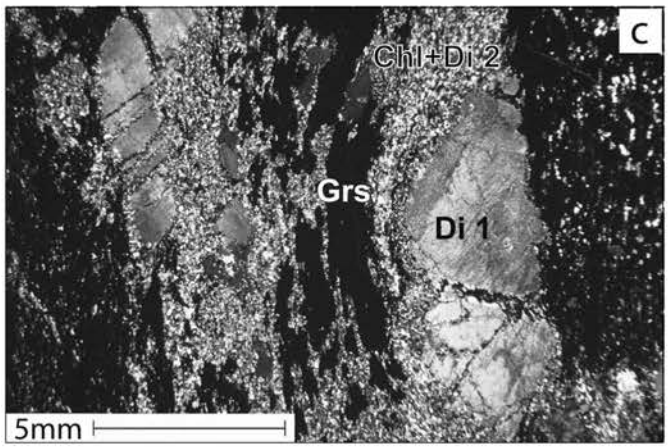

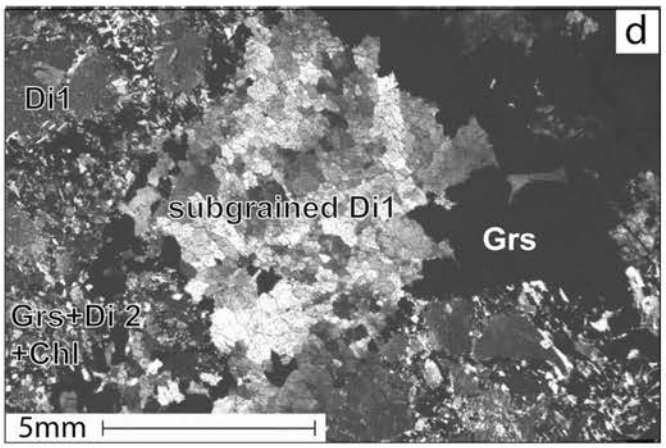

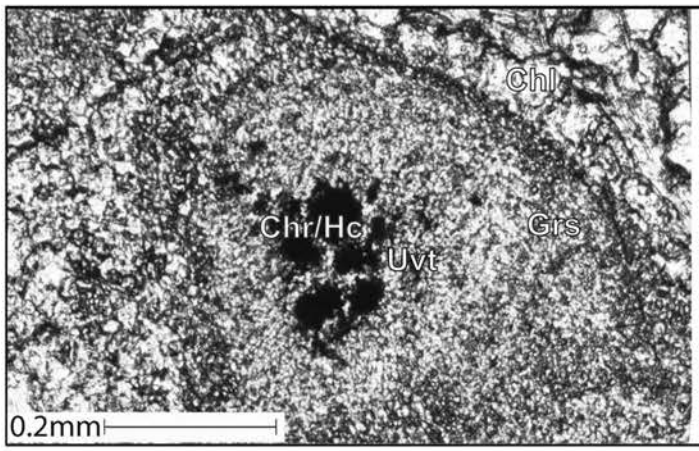

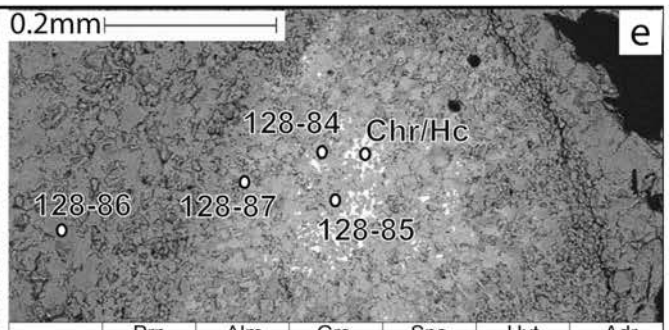

	Prp	Alm	Grs	Sps	Uvt	Adr
128-84	0.4%	2.0%	39.0%	0.0%	49.7%	8.2%
128-87	0.9%	0.8%	47.2%	0.5%	38.0%	12.1%
128-85	0.6%	1.2%	58.0%	0.3%	32.7%	7.2%
128-86	0.4%	1.8%	85.2%	0.2%	2.4%	10.0%

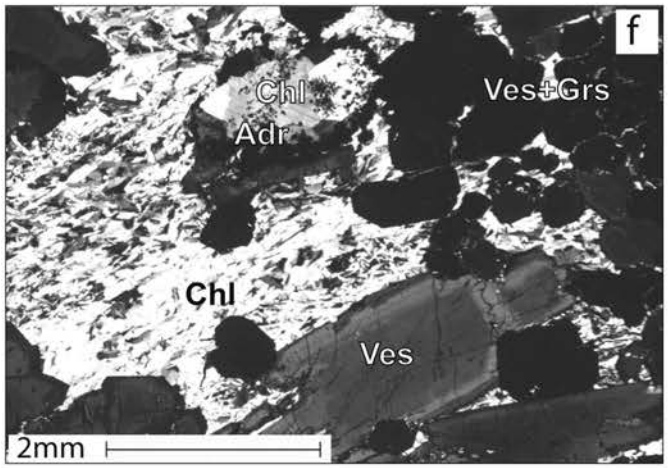

Fig. 6 - Photomicrographs of rodingites (abbreviations according to Siivola and Schmid, 2007). a) Garnet-rodingitic dykes: chlorite, garnet and minor diopside are the main components. b) BSE image and EDS analyses of sample AV91 (garnet-rodingitic dyke): chromite-hercynite series mineral surrounded by Cr-garnet. c) Sample AV143 (garnet-rodingitic dyke): diopside 1 surrounded by garnet layer and chlorite + diopside 2. d) Sample AV89 (garnet-rodingitic dyke): subgrained diopside 1 surrounded by garnet + chlorite + diopside 2. e) Sample AV128 (mixed garnet/vesuvianite-rodingitic dyke): chromite-hercynite series mineral surrounded by Cr-garnet (photomicrograph on the left; BSE image, and EDS analyses on the right). f) Sample AV129 (mixed garnet/vesuvianite-rodingitic dyke): zoned vesuvianite, chlorite and garnet. Andraditic garnet surrounds coarse-grained chlorite.

south of Gran Lac), that are also characterized by abundant titanite. Samples AV103 and AV105 also show Fe-rich-chlorite, classified on the basis of Hey (1954) as ripidolite, pycnochlorite, and clinochlore with high Fe values. Other minerals are epidote and allanite (mm-sized). Chlorite of other samples has a quite homogeneous composition with high Mg contents (clinochlore and rarely sheridanite and penninite). Pyroxene, when present, is diopside with high Mg and Ca contents and $X_{Mg}[Fe^{tot}] > 0.90$ (X_{Mg} $[Fe^{tot}]$ = Mg/(Mg + Fe^{tot}) molar). Only pyroxene from samples AV103 and AV105 is Na-diopside or omphacite (X_{Mg} $[Fe^{tot}]$ = 0.67-0.73; Table 2).

We finally studied two samples characterized by high diopside contents (sample AV89 near Gran Lac and sample AV143 near Lac Couverte, diopside-grossular-rodingitic dykes). These samples exhibit a different texture and modal composition with respect to other garnet-rodingites (diopside up to 65 vol.%, chlorite 5-25 vol.% and garnet 10-40 vol.%), but similar mineral compositions. These two samples contain mm-sized porphyroblasts of diopside (diopside 1, Fig. 6c), locally subgrained (Fig. 6d). A second-stage, fine-grained diopside (0.1 mm-sized diopside 2) pertains to the main rodingite assemblage (grossular, diopside, and chlorite) or it occurs in diopside-chlorite-layers interbedded with garnet layers.

Mixed garnet/vesuvianite-rodingitic dykes

Serpentinite near Cote Mouton and Tete des Hommes (see Fig. 2) contains abundant bimodal garnet-rich and vesuvianite-rich rodingitic dykes. Garnet-rich samples show petrographic features similar to those of garnet rodingitic dykes: garnet 60-80 vol.%, chlorite 20-40 vol.%, ± diopside. Grainsize ranges from 0.1 mm to 1 cm. Garnet contains grossular up to 96% and some Cr-rich-garnet (38-50% uvarovite, 39-48% grossular, 8-13% andradite) surrounding chromite-hercynite series mineral (Fig. 6e, Table 3). Chlorites are classified as clinochlore or sheridanite; diopside shows high Ca-Mg (X_{Mg} $[Fe^{tot}] > 0.95$) and low Fe-Na values. Locally we observed grossular crystals replaced by vesuvianite.

Other samples (e.g., sample AV129) exhibit petrographic features that are transitional between those of garnet-rich and vesuvianite-rich rodingites, being characterized by vesuvianite (40-50 vol.%), chlorite (20-30 vol.%), and garnet (20-30 vol.%). In these samples, vesuvianite is coarse-grained (2-4 mm in size), shows a concentric zonation (Fig. 6f) and quite homogeneous chemical composition (X_{Mg} $[Fe^{tot}]$ = 0.68-0.76). Mm-sized garnet is grossular (up to 97%), but we also analyzed Fe-Cr-rich garnet clusters (up to 40% andradite and 12% uvarovite) around large chlorite crystals (Fig. 6f). Chlorite shows low Fe and Si contents (clinochlore).

Vesuvianite-rich samples (e.g., sample AV134) are quite similar to vesuvianite rodingitic dykes and consist of mm-cm-sized vesuvianite (up to 95 vol.%), mm-sized chlorite (5-45 vol.%), and rare diopside. Vesuvianite is characterized by a large X_{Mg} range (X_{Mg} $[Fe^{tot}]$ = 0.62-0.79). Chlorite shows clinochlore composition. Diopside presents high Ca-Mg values (X_{Mg} $[Fe^{tot}] > 0.95$). Garnet presents high Ca and Fe values (andradite 60-80%).

Vesuvianite-rodingitic dykes

Yellow-green coloured rodingitic dykes consist of vesuvianite (50-95 vol.%), chlorite (5-45 vol.%), ± diopside (up to 15 vol.%), ± garnet (often concentrated in veins). Grainsize ranges from 0.1 mm (sample AV140) to 2 mm (sample AV130 and sample AV148). Chlorite and vesuvianite layers mark the rock foliation. Vesuvianite shows X_{Mg} $[Fe^{tot}]$ = 0.47-0.64. Chlorite is mainly classified as clinochlore, with minor penninite and sheridanite (low Fe and Si contents). Diopside is characterized by high Ca-Mg values (X_{Mg} $[Fe^{tot}]$ > 0.94). Some veins, up to 2 cm-thick and several-cm long, are filled with garnet, minor chlorite, diopside, and vesuvianite. Garnet shows high Ca contents (grossular > 86%). In contrast, garnet from the sample AV140 shows high Fe values (andradite > 63%). Vesuvianite grows around garnet and some coarse-grained vesuvianite veins cut garnet veins.

Foliated rodingites

The foliated rodingites at the contact between garnet-rodingitic dykes and serpentinites (sample AV127 and AV100) mainly consist of diopside (65-90 vol.%), chlorite

Table 3 - Representative EDS analyses of spinels (chromite-hercynite) in rodingite.

	Spinel	
	128-83	**127-1**
	Grossular rodingite	Foliated rodingite
SiO_2	0.2	0.5
Al_2O_3	4.9	4.7
Cr_2O_3	59.4	57.6
Fe_2O_3	2.0	3.4
TiO_2	0.0	0.0
V_2O_3	0.0	0.0
FeO	24.1	29.5
MnO	1.1	1.4
MgO	3.2	0.7
ZnO	2.5	1.3
NiO	0.0	0.0
CoO	0.0	0.0
Total	97.3	99.2
Ions of the basis of 4 O		
Si	0.0	0.0
Al	0.2	0.2
Cr	1.7	1.7
Fe^{3+}	0.1	0.1
Ti	0.0	0.0
V	0.0	0.0
Fe^{2+}	0.0	0.0
Sito R3	2.0	2.0
Fe^{2+}	0.7	0.9
Mn	0.0	0.0
Mg	0.2	0.0
Zn	0.1	0.0
Ni	0.0	0.0
Co	0.0	0.0
Sito R2	1.0	1.0
$R2_2TiO_4$	0.0	0.1
$R2Al_2O_4$	10.7	10.3
$R2Cr_2O_4$	86.6	84.9
$R2Fe_2O_4$	2.7	4.7

(10-25 vol.%), with minor garnet (up to 10 vol.%). Grain-size ranges from 0.05 to 0.5 mm. Diopside and chlorite layers are interbedded and mark a strong foliation (Fig. 7a), folded by at least two subsequent deformation phases. Chlorite shows high Mg values (clinochlore); diopside exhibits low Fe contents (X_{Mg} [Fe^{tot}] > 0.90). Near the chlorite-rich blackwall, garnet of the foliated rodingites shows high Ca contents (63-79% grossular) and locally high Cr values (39% grossular, 26% uvarovite and 22% andradite). In the latter case, Cr-rich garnet surrounds relics of chromite-hercynite series mineral (Table 3).

The foliated rodingites enclosing thin rodingitic dykes (e.g. sample AV93) are characterized by chlorite (40 vol.%), clinozoisite-zoisite (~ 30 vol.%), epidote (20 vol.%) and diopside (up to 10 vol.%). Foliation is here defined by chlorite cleavage domains and diopside-zoisite microlithons (Fig. 7b). Mm-sized epidote crystals are completely surrounded by the rock foliation.

Rodingitic reaction zones

The contact between serpentinites and metabasite pods is not usually rodingitized, but we locally observed evidence of rodingitization in Ca-amphibole rich metabasite samples (south of Gran Lac), where mm-sized diopside and calcite grow over the main mineral assemblage. Near the metabasite/serpentinite contact, we also recognized rodingitic reaction zones up to 10 m-thick and 50 m long (sample AV119). These metasomatic rocks consist of layers distinguished by different colours and mineral assemblages (Fig. 7c): reddish layers with 0.1-1 mm-sized crystals are made up of Ca-garnet (more than 50 vol.%), calcite (~ 20 vol.%), epidote (~ 10 vol.%), Ca-amphibole (~ 10 vol.%) and chlorite (~ 10 vol.%); green layers with mm-sized crystals consist of epidote (50-80 vol.%), diopside (~ 20 vol.%), calcite (up to 10 vol.%), Ca-amphibole (~ 5 vol.%), chlorite (~ 5 vol.%). Chlorite and amphibole also form the blackwall (sample AV118) between rodingite and serpentinite.

Garnet in both layer types shows high Ca and Fe values (grossular 50%, almandine 20-30%, andradite 10-20%). Locally, diopside has relatively high Na contents and may be classified as Na-diopside (Table 2). Fe^{tot} values of epidote are higher than 1.3 c.f.u.. Finally, chlorite is classified as pycnochlorite or diabantite (high Fe contents).

Pyroxene-epidote dykes

Samples AV124 and 125 consist of diopside (25-45 vol.%), clinozoisite-zoisite (20-60 vol.%) and chlorite (15-35 vol.%). Two different pyroxene generations occur (diopside 1 and diopside 2): coarse-grained diopside 1 (mm-sized crystals with mechanical twinning) is wrapped by foliation marked by fine grained chlorite, diopside 2 and clinozoisite-zoisite layers (Fig. 7d). Zoisite and clinozoisite show a textural equilibrium. Pyroxene presents homogeneous chemical compositions, with high Mg and Ca contents (X_{Mg} [Fe^{tot}] > 0.9), but we occasionally analyzed diopside 1 core with higher Al and Na contents (~ 10% of Jadeite). Chlorite is quite uniform in composition (clinochlore).

Pyroxene dykes

Two samples of pyroxene dykes (samples AV113 and AV138) show abundant coarse-grained diopside and a small amount of chlorite (less than 5 vol.%). Cm-sized pyroxenes define a pervasive foliation (Fig. 7e). The transition from the dyke to the mm-sized chloritic blackwall is sharp. Diopside shows high Mg and Ca contents (X_{Mg}[Fe^{tot}] ~ 0.95). Chlorite exhibits low Al and Fe contents (penninite).

Mineral composition summary

The EDS chemical analyses of main rodingitic minerals (chlorite, garnet, epidote, pyroxene, and vesuvianite) are summarized in the Tables 1 and 2 and represented by plots (Fig. 8), which compare the main rodingite types. Chlorite is classified on the basis of Hey (1954) and the analyses may be subdivided in three main groups (Fig. 8a):

– low-Si and low-Fe chlorite in garnet-, vesuvianite- and pyroxene-epidote rodingites (mostly low-Fe-clinochlore)
– low-Si and high-Fe chlorite of rodingitic reaction zone and Ca-Fe-garnet rodingites (high-Fe-clinochlore, ripidolite, pycnochlorite, and diabantite)
– high-Si and low-Fe chlorite of pyroxene rodingites and foliated rodingites.

Garnet analyses mark the difference between two main groups of rodingites. The first group includes rodingitic reaction zones and Fe-garnet rodingites. It is characterized by garnet with the lowest ugrandite (60-80%) and the highest almandine values (20-40%, Fig. 8b). The second group includes the other garnet rodingites, showing ugrandite-rich garnets. Garnet-rich rodingites show ugrandite composition trend from grossular to uvarovite (Fig. 8c). Differently, vesuvianite-rich rodingites show grossular-andradite trend (Fig. 8c).

Epidote mineral composition shows three main groups (Fig. 8d): Fe-epidote, Fe-rich clinozoisite, and Fe-poor-epidotes (clinozoisite and zoisite). Fe-epidote occurs in rodingitic reaction zones and Ca-Fe-garnet rodingites; Fe-rich clinozoisite is present in vesuvianite-rich and garnet-rich rodingites; clinozoisite and zoisite are contained in pyroxene-epidote dykes.

Pyroxene shows a quite uniform chemical composition, with very high Ca and Mg contents: the analyzed pyroxene crystals may be mostly classified as pure diopside with Wo percentages around 50%. Ca-Fe-garnet-rodingitic dykes and rodingitic reaction zones show pyroxenes with higher Na and Fe values, which are classified as Na-diopside or omphacite (Table 2).

Finally, we obtained vesuvianite analyses that show a large X_{Mg} and Al range (Fig. 8e). Different chemical compositions do not reflect any internal vesuvianite zonation. High-Fe vesuvianite crystals show purple anomalous interference colours, whereas low-Fe vesuvianites are brown-yellow.

DISCUSSION

Petrographic features and distribution of the Mount Avic rodingites are summarized in Table 4. The main mineralogical assemblage of the studied rocks is represented by ugranditic garnet + chlorite ± diopside ± epidote ± vesuvianite, but we also observed other mineral assemblages in the rodingitic dykes, as well as in foliated rodingites, and rodingitic reaction zones. Various assemblages and structures that characterize the Mount Avic rodingites are inferred to be related to the chemistry of the protolith (probably mafic dykes within serpentinite), to the extent of rodin-

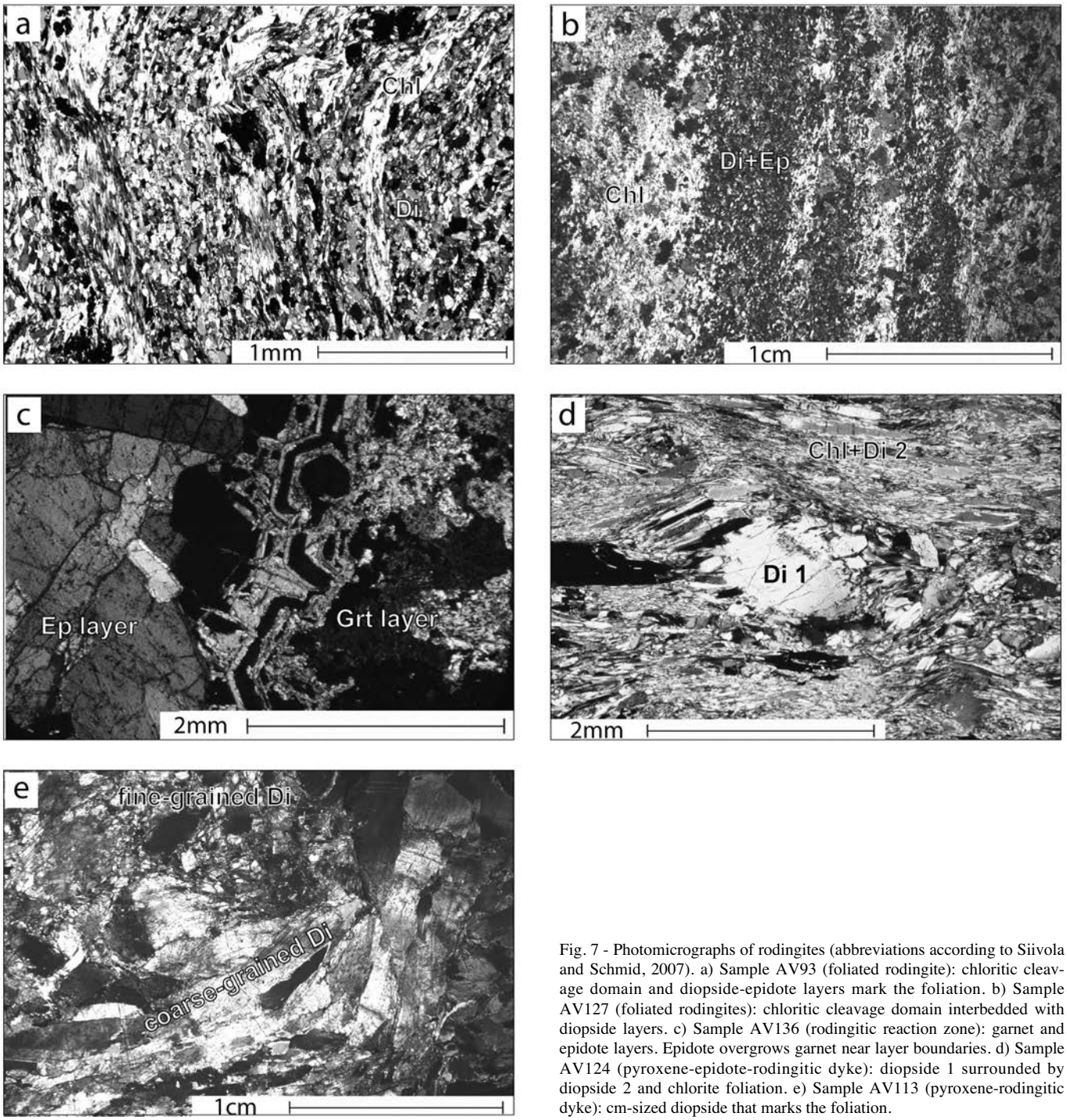

Fig. 7 - Photomicrographs of rodingites (abbreviations according to Siivola and Schmid, 2007). a) Sample AV93 (foliated rodingite): chloritic cleavage domain and diopside-epidote layers mark the foliation. b) Sample AV127 (foliated rodingites): chloritic cleavage domain interbedded with diopside layers. c) Sample AV136 (rodingitic reaction zone): garnet and epidote layers. Epidote overgrows garnet near layer boundaries. d) Sample AV124 (pyroxene-epidote-rodingitic dyke): diopside 1 surrounded by diopside 2 and chlorite foliation. e) Sample AV113 (pyroxene-rodingitic dyke): cm-sized diopside that marks the foliation.

gitization during oceanic serpentinization, and to the Alpine evolution (from HP metamorphism, to decompressional stage) that affected the Mount Avic massif as well as the Piemonte ophiolitic nappe.

In the following, the formation of different types of rodingites is discussed, and metamorphic reactions are proposed. All the metamorphic reactions reported in the following paragraphs are in part taken from the literature and in part suggested after modification from published works. All reactions are intended to be dependent on the composition, pressure and temperature of circulating fluids (Li et al., 2008).

Garnet-rodingitic dykes

In accord with Coleman (1967) garnet in rodingites grows from anorthite:

3 anorthite + Ca^{2+} + 2 H_2O → 2 clinozoisite + 2 H^+ (1a)

2 clinozoisite + 5 Ca^{2+} + 13 H_2O → 3 hydrogrossular + 1.5 SiO_2 + 10 H^+ (1b)

or

1.5 anorthite + 0.5 Ca^{2+} + 1.5 H_2O → prehnite + H^+ + 0.5 Al_2O_3 (1c)

prehnite + 4 Ca^{2+} + Al_2O_3 + 6 H_2O → 2 hydrogrossular + 8 H^+ (1d)

At the same time pyroxene and amphibole breakdown produces chlorite. By these reactions we can understand the

Table 4 - Petrographic features and distribution of rodingites from the Mount Avic serpentinites.

Occurrence (Sample #)	Textural relics	Metasomatic/metamorphic assemblage	Description	
Widespread	Chr/Hc, Ilm (?)	Grs, Chl, ± Di 2, ± Uvt, ± Ttn, ± Ep, ± Ves	Grossular-rodingitic dykes within serpentinite	Garnet-rodingitic dykes
Gran Lac (AV89), Lac Couvert (AV143)	Di 1	Di 2, Chl, Grs	Diopside-grossular-rodingitic dykes within serpentinite	
South of Gran Lac (AV103, AV105)	Aln	Grs/Alm, Chl, Omp, Ttn, ± Ep	Ca-Fe-garnet-rodingitic dykes within serpentinite	
Cote Mouton (AV130), north of Bec de Nona (AV140), west of Tete des Homes (AV148)	Chr/Hc	Ves, Chl, ± Di 2, ± Grs/Adr	Vesuvianite-rodingitic dykes within serpentinite and vesuvianite rodingite surrounding garnet-rodingitic dykes	
Gran Lac (AV100), Cote Mouton/Lac Leser (AV127)	Chr/Hc	Di 2, Chl, Grs, ± Grs/Uvt/Adr	Foliated rodingites between garnet-rodingitic dykes and serpentinite	
South of Lac Cornue (AV118)		Grs, Cal, Ep, Ca-am, Chl Ep, Di, Cal, Ca-am, Chl	Rodingitic reaction zones (reddish and green layers) between metabasite and serpentinite	
Cote Mouton (AV124, AV125)	Di 1	Di 2, Zo/Czo, Chl	Pyroxene-epidote dykes within serpentinite	
North of Pisonet (AV113), Col de Lac Blanc (AV138)		Di (1 or 2?), Chl	Pyroxene dykes within serpentinite	

Abbreviations according to Siivola and Schmid (2007).

evolution from a gabbroic/dioritic protolith to a rodingitic assemblage with hydrogrossular and chlorite, but the Mount Avic garnet-rodingites often show a more complex assemblage and garnet is always grossular instead of hydrogrossular.

Grossular-rodingitic dykes

Rodingites with garnet characterized by high grossular contents are the most widespread in the world (Table 5). The main assemblage of these rocks, similar to grossular-rodingitic dykes from Mount Avic, is quite uniform in the Archean - Paleoproterozoic mafic-ultramafic sequences, in both metamorphosed and un-metamorphosed ophiolitic complexes. The protolith is generally a mafic rock (gabbro, diorite or basalts). The analyzed samples from Mount Avic display some textural relics that may be interpreted as pre-metasomatic minerals. Similar relics occur in the rodingites from the Vumba Schist Belt in Botswana (Mogessie and Rammlmair, 1994). Chromite/hercynite series minerals, surrounded by uvarovite rich garnet (see Fig. 6b), could be interpreted as due to the following reaction, modified after Mogessie and Rammlmair (1994):

Al-Fe-ugrandite + chromite → Cr-Al-Fe-ugrandite + chromite-hercynite (2)

Textures and mineral chemistry suggest an Al-Cr exchange between ugranditic garnet and spinel during this reaction (Al-Fe-ugrandite + Cr = Cr-Al-Fe-ugrandite + Al; chromite + Al = chromite-hercynite + Cr). Chromite represents the magmatic relic of the rodingite protolith. Uvarovitic garnet could have grown during a metasomatic event, at the same time or after grossular-andradite crystallization.

The main rodingitic assemblage (ugranditic garnet, chlorite, ± diopside 1, ± diopside 2, ± epidote) probably grew during an early oceanic metasomatic event (at the same time of uvarovite) according to the reaction proposed by Hatzipanagiotou et al. (2003):

16 clinozoisite + 3 tremolite + 25 CaO + H_2O →
3 clinochlore + 21 grossular (3)

after clinozoisite of reaction (1a). Tremolite may be a product of pyroxene/amphibole breakdown.

The occurrence of epidote is related to reaction

5 prehnite → 2 epidote + 2 grossular + 3 SiO_2 + 4H_2O (4)

proposed by Honnorez and Kirst (1975) and based on prehnite of reaction (1c). An alternative reaction is suggested by Mogessie and Rammlmair (1994):

4 anorthite + clinopyroxene + 2 H_2O + Ca^{2+} → epidote + grossular + zoisite + SiO_2 + 2 H^+ (5)

Diopside 2 abundance is strictly related to diopside 1 content. The observed textures suggest that diopside 2 is the product of diopside 1 dynamic recrystallization, probably developed during the early Alpine evolution. So, diopside 1 could have grown during oceanic rodingitization, while diopside 2 is the product of recrystallization during the Alpine deformation.

Diopside-grossular-rodingitic dykes

Diopside rich rodingites, everywhere showing grossular or andradite (Table 6), are less widespread than grossular-rodingites, but they crop out in the Archean - Paleoproterozoic mafic-ultramafic sequences, in the metamorphosed and un-metamorphosed ophiolitic complexes. Chlorite, epidote, and vesuvianite are often reported. Protoliths are invariably mafic rocks and some authors report diopside as a magmatic relic (Dal Piaz et al., 1980).

In the diopside-grossular-rodingitic dykes from Mount Avic, diopside 1 porphyroblasts, locally subgrained, are textural relics (Figs, 6c, d, and 7a), surrounded by main rodingite assemblage. Diopside 1 crystals probably are textural relics of magmatic clinopyroxene that have been Ca-enriched and Fe-depleted during the first metasomatic stage, according to the qualitative reaction modified after Li et al. (2008):

plagioclase + clinopyroxene + H_2O + Ca^{2+} → grossular + chlorite + diopside (6)

Diopside 2, as in the grossular-rodingites, is the product of diopside 1 recrystallization during Alpine evolution. Grossular, chlorite, and epidote growth follows reactions (3), (4), and (5).

Ca-Fe-garnet-rodingitic dykes

Garnet rodingitic dykes with high Fe contents have not been reported in previous rodingite studies. The reactions that produced the metasomatic assemblage were probably the same of grossular-rodingites, but the protolith is quite differ-

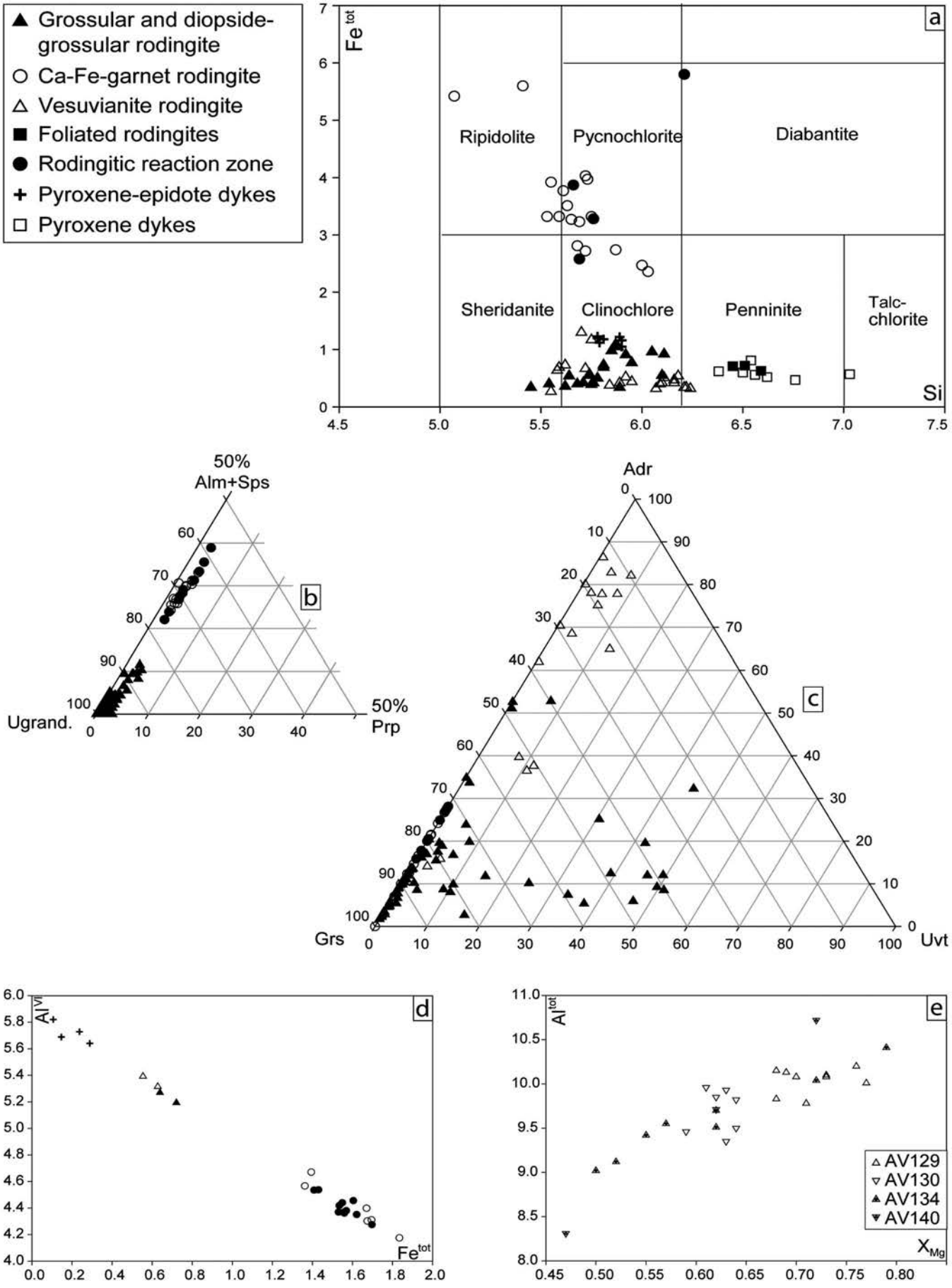

Fig. 8 - Composition plots of rodingite minerals. a) Chlorites classification (Hey, 1954) on the basis of 28 O recalculation. Analyzed chlorites from rodingites and chlorite-rich blackwalls are not distinguished. b-c) Garnet classification on the basis of 12 O recalculation. d) Fe_{tot} - Al^{VI} plot for epidote on the basis of 25 O recalculation. e) X_{Mg} - Al_{tot} vesuvianite plot on the basis of 50 cations recalculation. Abbreviations according to Siivola and Schmid (2007).

Table 5 - Summary of (hydro)grossular-rodingites reported in literature, similar to Mount Avic rodingitic dykes.

Reference	Occurrence	Igneous assemblage (Protolith)	Metasomatic/metamorphic assemblage	Description
(Baltatzis, 1984)	Skiros island, Greece		Grs, Chl, Ves	Rodingite lens within serpentinite
(Bamba et al., 1969)	Nukabira mine, Hokkaido, Japan		Grs, Cr-Grt	Rodingite in serpentinite
(Bloxam, 1954)	Girvan-Ballantrae complex, Ayrshire	Pl, Px (Gabbro)	Grs, hydro-Grt, Zo, Prh, Chl, Cal, Pectolite	Altered and garnetized gabbro in serpentinite
(Christidis et al., 1998)	Vourinos ophiolite complex		Hydro-Grs, Ves, Ep, Chl, Srp	Rodingite dykes in serpentinized harzburgite with chromite ore
(Coleman, 1966)	Dun Mountain (New Zealand))	Hbl, Aug (Gabbro)	Hydro-Grs, Di, Chl, Ves, Prh	Rodingite within serpentinite
	Whangamoa Area (New Zealand)	(Gabbro)	Hydro-Grs Chl	Rodingite within serpentinite
	Silverdale-Wellsford Area (New Zealand)	(Gabbro)	Hydro-Grs, Prh, Chl	Rodingite within serpentinite
	USA Westren Coast (Oregon)	(Gabbro, dacite)	Hydro-Grt, Ves, Chl, Di, Ttn	Rodingite within serpentinite
(Coleman, 1967)	USA Western Coast (California)	(Gabbro)	Hydro-Grt, Di, Prh, Ttn	Rodingite within serpentinite
	USA Western Coast (Washington)	(Gabbro)	Hydro-Grt, Di, Aug	Rodingite within serpentinite
(Dal Piaz, 1969)	Givoletto, Lanzo, W Alps. Italy	Pl, Di (Gabbro)	Grs, Chl	Rodingitic gabbro dykes within serpentinite
(Dal Piaz, 1969)	Valle d'Ayas, NW Alps, Italy	Aug (Gabbro)	Grs, Chl	Rodingitic gabbro dykes within serpentinite
(Dubinska et al., 2004a)	Lower Silesia, Poland		Grs, opal	Grs-rodingite in serpentinite massif
(Dubinska et al., 2004b)	Jordanow-Gogolow Bohemian Massif, Poland	Ab, Ap	Grs, Czo, Zo, Ttn, An Di, Czo, Chl, Prh	Rodingite boudins within serpentinite
(Flinn, 1999)	Vord Hill Klippe, Shetland Ophiolite,		Grt, Di, Ep, Prh	Rodingite bodies within metadunite lenses
(Grange, 1927)	Nelson, Dun Mountain, New Zealand	Pl, Px (Gabbro)	Grs, Di	Rodingitized gabbro in serpentine
(Hatzipanagiotou and Tsikouras, 2001)	Samothraki Ophiolite, NE Aegean, Greece	(Diorite)	Grs/Adr, Ves, Di, Ep, Cal, Prh	Rodingite boudins and pods within serpentinite
(Li et al., 2004; Li et al., 2008)	Zermatt, Zermatt-Saas Ophiolites, CH	Cpx (Basalt)	hydro-Grs, Ves, Chl, Di, Czo/Ep	"Rodingite I" within serpentinite
(Li et al., 2004; Li et al., 2008)	Zermatt, Zermatt-Saas Ophiolites, CH	Cpx (Basalt)	Hydro-Grs, Ves, hydro-Adr, Chl, Di, Cal, Ep	"Rodingite II" within serpentinite
(Li et al., 2007)	Western Tianshan, China	(Eclogite)	Hydro-Grs, Di, Chl, Ep, Ves	Hydrogrossular-diopside-rodingite
(Mittwede and Schandl, 1992)	Appalachian Piedmont, South Carolina, USA	Di, Am (deformed Gabbro)	Grs/Adr, Ep	Coarse-grained rodingite
(Mogessie and Rammlmair, 1994)	Vumba Schist Belt, Botswana, Africa	Chr (Gabbro)	Grs, Ep/Zo, Di, Qz, Ttn	Rodingite within serpentinite
(Normand and Williams-Jones, 2007)	JM asbestos mine, Asbestos, Quebec	(Diorite)	Grs, Cpx, Chl, Zo, Prh, Ab, Kfs, Ves	Rodingitized diorite within serpentinite
(Normand and Williams-Jones, 2007)	JM asbestos mine, Asbestos, Quebec	(Granite)	Grs, Chl, Cpx, Prh, hydro-Grs, Ves, Zo, Wo	Rodingitized granite within serpentinite
(Ortiz-Hernández, 1999)	Sierra de Guanajuato, Mexico	Pl, Cpx, Ap (Gabbro)	Para-Grt, hydro-Grs, Ves, Ep, Prh, Di, Mg-Hbl, Chl, Tobermorite, Gyrolite	Rodingitized gabbro within serpentinite
(Puga et al., 1999)	Mulhacen Complex, SE Spain	(Dolerite)	Grs, Di, Ca-Am, Chl, Ttn, Ep,	Metarodingite within serpentinite
(Puschnig, 2002)	Valmalenco, Italy	(Basalt)	Grs, Ves, Chl, Di, Ep, Cal	Metarodingites within ultrabasic rocks
(Qaiser et al., 1970)	Naranji Sar, Malakand, West Pakistan		Grs, Ves, Opx, Srp, Chl, Mag, Chr	Rodingitic dykes within serpentinite
(Scarrow et al., 1999)	Mindyak, Southern Urals	(Gabbro)	Grs, Di, Ca-Am, Rt, Ilm, Ap, Ttn, Zrn	Garnet metagabbros in serpentinized peridotite
(Schandl et al., 1990)	Bowman asbestos mine, Ontario	(Gabbro)	Hydro-Grs, Di	Rodingitized gabbro in serpentinized ultramafic rocks

Abbreviations according to Siivola and Schmid (2007).

Table 6 - Summary of various kinds of rodingites reported in literature, similar to Mount Avic rodingitic dykes.

Reference	Occurrence	Igneous assemblage (Protolith)	Metasomatic/metamorphic assemblage	Description
Diopside-grossular-rodingites				
(Dal Piaz et al., 1980)	Valtournanche, Western Alps, Italy	Di (Gabbro)	Di, Grs/Adr, Ep, Chl, Ves	Rodingitic gabbro dykes within serpentinite
(Evans et al., 1979; Evans et al., 1981)	Cima di Gagnone, Central Alps, CH	(Gabbro, basalt)	Di, Grs/Adr, Ep, Hbl, Ves, Chl, Clintonite, Ttn, Prv, Ti-Adr,	Rodingite boudin and layer in ultramafic schists (serpentinite)
(Grice and Gasparrini, 1981)	Jeffrey Mine, Quebec		Di, Grs, Ves, Serpentiniite	Rodingite dyke within serpentinized dunite
(Hatzipanagiotou et al., 2003)	Lesvos island, NE Aegean, Greece	(Gabbro)	Di, Grs, Ep/Czo, Chl, Vuagnatite	Rodingitized dykes
(Mogessie and Rammlmair, 1994)	Vumba Schist Belt, Botswana, Africa	(Gabbro)	Di, Ep, Grs/Uvt, Chr, pl, Qz	Rodingite within serpentinite
(Puga et al., 1999)	Mulhacen Complex, SE Spain	(Dolerite)	Di, Grt (pyralspite)	Partly amphibolitized "eclo-rodingites"
(Schandl et al., 1989)	Abitibi Greenstone Belt, Ontario, Canada	(Gabbro, diabase, pyroxenite, lamprophyric andesite)	Di, hydro-Grs, Ep, Prh, Tr, Ves, Ttn, Chl, Phl	Rodingites within serpentinized ultramafic rocks
Vesuvianite-rodingites				
(Dubinska and Wiewiora, 1999)	Przemilow, Bohemian Massif, Poland	Di	Ves, Chl/Vrm, Ap, Zrn	Rodingite/metarodingite boudins within serpentinite
(Dubinska et al., 2004a)	Lower Silesia, Poland	Cpx	Ves, Grs, Adr, Ep, Phl	Ves-rodingite in serpentinite massif
(Honnorez and Kirst, 1975)	Verna and Romanche fracture zones, Mid-Atlantic Ridge	Di/Aug, Ilm, Ap, Pl (Gabbronorite)	Ves, hydro-Grs, Prh, Ep, Ttn, Chl, Srp, Cb, Di	Rodingite
(Li et al., 2004; Li et al., 2008)	Zermatt, Zermatt-Saas Ophiolites, CH		Chl, Ves, hydro-Adr,	"Rodingite III" within serpentinite
(Li et al., 2007)	Western Tianshan, China	(Eclogite)	Ves, Chl, hydro-Grs, Di	Vesuvianite-rodingite
(Normand and Williams-Jones, 2007)	JM asbestos mine, Asbestos, Quebec		Ves, Cpx	Vesuvianite-rich veins
Epidote-rich-rodingites				
(Dubinska et al., 2004a)	Lower Silesia, Poland	Ab, Ap, Zrn	Czo, Grs, Chl, Di, Afs, Prh, Ttn	Czo-rodingite in serpentinite massif
(Dubinska et al., 2004a)	Lower Silesia, Poland	Di	Ep, Grs, Clintonite, Spl, Di, Am	Clintonite-rodingite in serpentinite massif
(Mittwede and Schandl, 1992)	Appalachian Piedmont, South Carolina, USA	Pl, Qz, Cpx, Am (sedimentary rocks)	Ep, Qz, Chl, Ttn	Fine-grained rodingite
(O'Hanley et al., 1992)	Cassiar, British Columbia, Canada		Czo, Tr, Prh, Grs, Di,	Fine-grained rodingite within serpentinite
(Attoh et al., 2006)	Dixcove greenstone belt, SW Ghana	Pl	Ep, Zo, Act, Chl	Rodingite blocks and pods within serpentinized ultramafic rocks
(Hatzipanagiotou and Tsikouras, 2001)	Samothraki Ophiolite, NE Aegean, Greece	(Diorite)	Ep, Cal, Di, Prh, Chl, Ab	Rodingite boudins and pods within serpentinite
Rodingitic reaction zones				
(Dal Piaz, 1969)	Cogne, NW Alps, Italy	(Marble with silicates)	Grs, Di, Ep, Wo, Act, Chl, Mag	Rodingitic reaction zones
(Dal Piaz, 1969)	Balangero, W Alps, Italy	Ttn, Ap, Zrn	Grs, Di	Rodingitic reaction zones
(Dal Piaz, 1969)	Montjovet, NW Alps, Italy	(Marble with silicates)	Ep, Zo, Di, Tr, Grt, Qz, Ab	Rodingitic reaction zones
(Leblanc and Lbouabi, 1988)	Bou Azzer, Morocco	Pl, Bt, Qz, Zrn, Ap, Ttn, Aln	Grt, Cpx, Ep, Prh, Cal, Ca- Am, Chl, Ab, Kfs	Rodingite along serpentinite/quartz diorite contact
(Normand and Williams-Jones, 2007)	JM asbestos mine, Asbestos, Quebec	(Slate)	hydro-Grs, Zo, Cpx, Prh, Grs	Rodingitized slate in thrust contact with serpentinite

Abbreviations according to Siivola and Schmid (2007).

ent. Ca-Fe-garnet-rodingitic dykes (samples AV103 and AV105) crop out close to a Ca-Na-amphibole metabasite body with eclogitic relics (see Figs. 2 and 4): we suggest that Ca-Fe-garnet-rodingitic dykes as well as metabasite with Ca-Na-amphibole derive from similar Fe-rich mafic rocks. The rodingitic dykes and the metabasite show mineral assemblages that highlight their HP Alpine evolution. However, the occurrence of HP, Ca-rich mineral assemblage (grossular-almandine, omphacite or Na-diopside) has been recorded only within the dykes and not in the nearby metabasite body. This evidence suggests that dykes have been metasomatized before the subduction-related metamorphic peak, while the metabasite suffered the HP Alpine evolution without rodingitization. We thus infer that grossular-almandine, omphacite or Na-diopside represent the products of Alpine recrystallization of a previous mineral assemblage affected by oceanic metasomatism. A similar evolution has been suggested by Bocchio et al. (2000) for rodingitized Fe-Ti-metagabbros of the Aosta Valley and Soana Valley (Piemonte).

Vesuvianite-rodingites

Vesuvianite-rich-rodingites were reported in metamorphosed and un-metamorphosed mafic complexes (Table 6), as well as in rodingitic veins dragged along the Middle Atlantic Ridge (Honnorez and Kirst, 1975). Vesuvianite-rodingites also show chlorite, garnet, epidote and clinopyroxene.

In the Mount Avic massif, vesuvianite often occurs at the rims of garnet-rodingitic dykes and petrographic observations suggest the crystallization of vesuvianite from garnet. The vesuvianite-rodingites also show textural relics similar to those of grossular rodingites (chromite/hercynite series minerals, surrounded by uvarovitic garnet, see Fig. 6e).

On the basis of the observed structures, textures and mineral assemblages, we suggest the following qualitative reactions, modified after Li et al. (2008), for vesuvianite crystallization:

$$\text{grossular} + \text{chlorite} + H_2O \rightarrow \text{vesuvianite} + SiO_2 \quad (6a)$$

$$\text{grossular} + \text{diopside} + H_2O \rightarrow \text{vesuvianite} + \text{chlorite} + SiO_2 \quad (6b)$$

These reactions do not need Ca supplies (typical of oceanic metasomatism), so vesuvianite may be a metamorphic Alpine product. Li et al. (2008) highlight that all the reactions producing vesuvianite in the ZS ophiolites could have been developed during the Alpine evolution. According to these authors, reaction (6a) may be referred to early Alpine metamorphism (about 400°C and 1.5 Gpa); reaction (6b) probably took place during the ophiolite uplift and late Alpine metamorphism (about 500°C and 1 Gpa).

Foliated rodingites

In this paper foliated rodingites near garnet-rodingites are reported for the first time. The assemblage is similar to that of some grossular-rodingitic dykes, but we also observed chromite/hercynite relics, surrounded by uvarovite and Ca-Cr-garnet. Foliated rodingites may represent lenses of strongly deformed garnet-rodingites. Alpine deformation produced mineralogical layering and strong recrystallization of diopside 1 in fine-grained diopside 2.

Rodingitic reaction zones

Rodingitic reaction zones are reported in most of the ophiolitic massifs from the Alps (Table 6), often occurring between metasedimentary rocks and serpentinite. In the Mount Avic massif we report for the first time a rodingitic reaction zone between serpentinite and metabasite pods. This reaction zone shows structural and petrographic features similar to those found in a reaction zone from Balangero quarry (Dal Piaz, 1969). The Balangero reaction zone occurs at the contact between serpentinite and gneiss/micaschist and shows garnet-rich-layers interbedded with diopside-rich-levels, similarly to the Mount Avic rodingitic reaction zone. This similarity suggests that locally the rodingite mineral assemblage may be related to Ca-rich fluid composition more than to the protolith composition, probably reflecting high fluid/rock ratios.

Pyroxene-epidote and pyroxene dykes

Epidote-rich-rodingites are reported from many mafic complexes (Table 6), but not from Alpine ophiolites. Moreover, pyroxene-epidote-dykes from Mount Avic are quite different from other epidote-rich-rodingites reported in literature, because of the lack of garnet and prehnite and the high modal contents of diopside. However, we highlight some petrographic similarities between the Mount Avic pyroxene-epidote rodingites and metasomatic rocks from Samothraki Ophiolite (Hatzipanagiotou and Tsikouras, 2001 - Table 6), for which these authors suggest a dioritic protolith.

Pyroxene-epidote dykes display an unusual mineral assemblage, reported here for the first time, even though they show the same structure of other rodingitic dykes as well as a mm-sized chloritic blackwall.

SUMMARY AND CONCLUSIONS

The Mount Avic massif mainly consists of serpentinites including mafic and metasomatic rocks. Following Tartarotti et al. (1998), this mafic/ultramafic part of the ophiolitic sequence was a mantle fragment exposed on the Tethys ocean floor before subduction. Metabasites and rodingites are interpreted as deriving, respectively, from gabbroic bodies and dykes that intruded mantle rocks. On the other hand, the lack of a continuous gabbroic layer and a dominant mantle ultramafic component, has been also observed for the Northern Apennine ophiolites (Tribuzio et al., 2000). The Mount Avic and Northern Apennine lithosphere sections fit well the slow-spreading ridge model of discontinuous magmatic crust (e.g. Cannat, 1993; Lagabrielle et al., 1998).

Fieldwork, petrographic studies, and EDS analyses of the Mount Avic rodingites allow to recognize some peculiar features of these metasomatic rocks. Rodingites occur as boudinaged and folded dykes, up to 2m- thick and several meters- long, within the serpentinite massif and are always surrounded by a chlorite-rich blackwall. Rodingitic dykes mostly consist of ugranditic garnet, chlorite ± diopside ± epidote ± vesuvianite, but we also recognized other mineral assemblages (vesuvianite-chlorite-, diopside-epidote-chlorite-, diopside-chlorite-rodingitic dykes) as well as foliated rodingites and rodingitic reaction zones.

Mineral chemistry analyses of chlorite, garnet, and epidote indicate the presence of Fe-rich and Fe-poor rodingites, most probably due to different protoliths. Rodingitic reaction zones and Ca-Fe-garnet rodingites exhibit chlorite, garnet and epidote with the highest Fe values and pyroxene with high Fe and Na contents, probably due to a Fe-Na-rich

protolith. Grossular- and vesuvianite-rich rodingites (the most common rodingite type) show chlorite, garnet and epidote with lower Fe values: similar rodingites reported in literature are often interpreted as deriving from Mg-rich gabbros. Pyroxene-epidote and pyroxene dykes are also made of minerals with low Fe values. The spatial distribution of Fe-rich-rodingites reflects that of outcrops of Ca-Na-rich amphibole metabasites and eclogites. On the basis of this evidence we propose that Fe-rich-rodingites as well as metabasite with Ca-Na-amphibole derive from the same Fe-rich mafic rock. Both rodingitized dykes and Fe-rich mafic body recrystallized during the Alpine metamorphism.

The observed mineral associations cannot be undoubtedly attributed to the oceanic or orogenic hystory because rodingitic assemblages are not pressure-sensitive (see also discussion in Li et al., 2008). However, analyses of garnet- and vesuvianite-rodingites, as well as of foliated rodingites, allow us to identify relics of several evolution stages. 1) Chromite/hercynite series minerals, surrounded by uvarovite and Ca-Cr-garnet, are interpreted as magmatic relics. 2) Diopside 1 porphyroblast could be a relic of oceanic rodingitization, before the Alpine deformation. Diopside 1 probably grew at the same time of the main mineralogical assemblage (ugranditic garnet + chlorite ± epidote). 3) Alpine deformation produced diopside 1 subgrain and recrystallization into diopside 2 as well as garnet-chlorite recrystallization.

Vesuvianite may be an Alpine product from grossular-rodingite assemblage (according to Li et al., 2008). Vesuvianite-rich rodingites are typical of metamorphosed serpentinitic complexes (Dubinska and Wiewiora, 1999; Dubinska et al., 2004a; Li et al., 2004; 2007; 2008), while not metamorphosed ophiolites and the modern oceanic crust show only vesuvianite veins and restricted vesuvianite bodies (Honnorez and Kirst, 1975). We hypothesize that vesuvianite rodingites grew on the previous main rodingite assemblage (garnet, chlorite) during early Alpine metamorphism following reaction (6a). The large water supply, necessary to vesuvianite crystallization, may be derived from chlorite blackwall and surrounding serpentinite.

Finally, we observed that metabasite pods are not metasomatized and a selective rodingitization affects only dykes. These features have suggested a speculative genetic model illustrated in Fig. 9. Following the model of a discontinuous magmatic crust, as proposed for the Jurassic Ligurian Tethys by Tribuzio et al. (2000), we envisage the occurrence of relatively small mafic bodies intruded in a mantle peridotite (partially serpentinized) exposed on the ocean floor. Intrusion and magmatic evolution also produced mafic dykes (Fig. 9a). Macro- and micro-fractures as well as faults, related to extensional tectonics in a spreading regime, allowed fluids circulation that supports serpentinization of the peridotite and rodingitization of mafic dykes (Fig. 9b). A cracking front developed in the oceanic lithosphere likely represented the lower limit of rodingitization, i.e. the deepest penetration of metasomatic Ca-rich fluids. The cracking front, which controls the distribution of metasomatism reactions, may have only partially affected the mafic bodies which are in fact scarcely or not rodingitized (Fig. 9c). After the oceanic evolution, the Mount Avic lithosphere was involved into the Alpine subduction. Serpentinites, mafic bodies and rodingite dykes were subsequently affected by HP metamorphism that yielded recrystallization of the oceanic rodingite assemblages and formation of new vesuvianite.

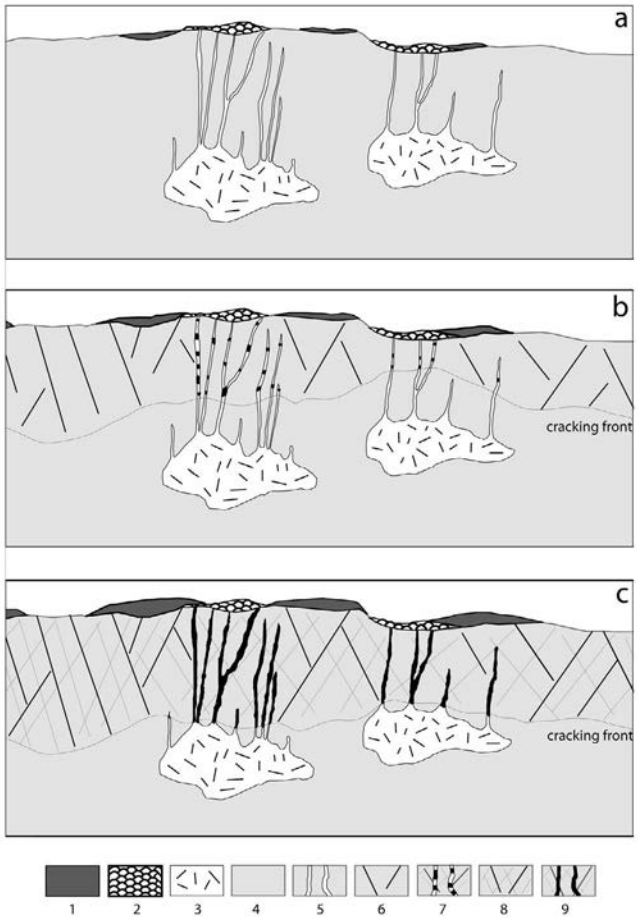

Fig. 9 - Cartoon showing the proposed model for the oceanic evolution of the Mount Avic rodingitic dykes (not on scale). a) Mafic bodies intrude the mantle peridotite or partially serpentinized peridotite. The emplacement is associated with dykes formation. b) Macro- and micro-fractures as well as faults support the fluid circulation that allows serpentinization and rodingitization event. c) Ca-rich fluid may saturate the oceanic lithosphere over a cracking front and produce a complete rodingitization of the dykes. 1) Sedimentary cover. 2) Basalt flows, 3) Mafic bodies. 4) Peridotite or partially serpentinized peridotite. 5) Mafic dykes. 6) Macro-fractures and faults in the serpentinized peridotite. 7) Partially rodingitized dykes. 8) Macro- and micro-fractures in the serpentinized peridotite. 9) Rodingitized dykes.

ACKNOWLEDGMENTS

The authors are grateful to J. Honnorez and B. Tsikouras for reviewing and commenting the earlier version of the manuscript. We appreciate revision and comments by A. Montanini that greatly improved the text. This study was supported by FIRST 2004 provided by Università degli Studi di Milano.

REFERENCES

Anhaeusser C.R., 1978. Rodingite occurrences in some Archaean ultramafic complexes in the Barberton Mountain Land, South Africa. Precamb. Res., 8 (1-2): 49-76.

Attoh K., Evans M.J. and Bickford M.E., 2006. Geochemistry of an ultramafic-rodingite rock association in the Paleoproterozoic Dixcove greenstone belt, southwestern Ghana. J. Afr. Earth Sci., 45 (3): 333-346.

Baldelli C., Dal Piaz G.V. and Lombardo B., 1985. Ophiolite eclogites from Verres, Val d'Aosta, Western Alps, Italy. Chem. Geol., 50 (1-3): 87-98.

Ballévre M., Kienast J.R. and Vuichard J.P., 1986. La "nappe de la Dent-Blanche" (Alpes Occidentales): deux unités austroalpines indépendantes. Ecl. Geol. Helv., 79 (1): 57-74.

Ballévre M. and Merle O., 1993. The Combin fault: compressional reactivation of a Late Cretaceous - Early Tertiary detachment fault in the Western Alps. Schweiz. Mineral. Petrogr. Mitteil., 73 (2): 205-228.

Baltatzis E., 1984. A new occurrence of rodingite from Skiros Island, Greece. N. Jahr. Mineral., Monats., 7: 317-322.

Bamba T., Yagi K. and Maeda K., 1969. Chrome garnet fron the vicinity of Nukabira mine, Hidaka province, Hokkaido, Japan. Proceed, Japan Acad., 45 (2): 109-114.

Barnicoat A.C. and Fry N., 1986. High -pressure metamorphism of the Zermatt-Saas ophiolite, Switzerland. J. Geol. Soc. London, 143 (4): 607-618.

Bearth P., 1967. Die ophiolite der Zone von Zermatt-Sass Fee. Geol. Karte Schwiez. N.F., 132: 1-130.

Bell J., Clark E. and Marshall P., 1911. The geology of the Sun Mountain subdivision, Nelson. N. Zealand Geol. Surv. Bull., 12: 1-71.

Benciolini L., Lombardo B. and Martin S., 1988. Mineral chemistry and Fe/ Mg exchange geothermometry of ferrogabbro-derived eclogites from the northwestern Alps. N. Jahr. Mineral., 159 (2): 199-222.

Bloxam T.W., 1954. Rodingite from the Girvan-Ballantrae complex, Ayrshire. Mineral. Mag., 30 (227): 525-528.

Bocchio R., Benciolini L., Martin S. and Tartarotti P., 2000. Geochemistry of eclogitised Fe-Ti-gabbros from various lithological settings (Aosta Valley ophiolites, Italian western Alps). Protolith composition and eclogitic paragenesis. Period. Mineral., 69 (3): 217-237.

Bowtell S.A., 1991. Sm-Nd and K-Ar dating of the Zermatt-Saas Fee Ophiolite, Western Alps. Terra Abstr., 3 (1): 96.

Bucher K., Fazis Y., De Capitani C. and Grapes R., 2005. Blueschists, eclogites, and decompressional assemblages of the Zermatt-Saas ophiolites: high-pressure metamorphism of subducted Tethys lithosphere. Am. Mineral., 90 (5-6): 821-835.

Buscemi S., 2003. Le epidositi e i metagabbri ofiolitici del settore meridionale del Monte Avic (Valle d'Aosta): studio geologico-strutturale e geochimico. Master Thesis, Univ. Studi Milano, 111 pp.

Caby R., Kienast J.R. and Saliot P., 1978. Structure, métamorphisme et modèle d'évolution tectonique des Alpes occidentales. Rev. Géogr. Phys. Géol. Dyn., 20 (4): 307-322.

Campari E., Portera F., Tartarotti P. and Spalla M.I., 2004. The Rifelberg-Garten Unit in the eclogitic ophiolites of the Upper Valtournanche (Piedmont Zone, Northwestern Italian Alps). 32nd IGC, Florence (Italy). Abstr. Vol., p. 294.

Cannat M., 1993. Emplacement of mantle rocks in the seafloor at mid-ocean ridges. J. Geophys. Res., 98 (3): 4163-4172.

Castelli D., 1985. La Falda Piemontese alla base del margine sudoccidentale del lembo dell' Emilius-Media Valle d'Aosta - Translated Title: The Piemonte Nappe underlying the southwestern margin of the Mt. Emilus Klippe-Middle Aosta Valley. Ofioliti, 10 (1): 19.34.

Chinner G.A. and Dixon J.E., 1973. Some high pressure parageneses of the Allalin gabbro, Valais, Switzerland. J. Petrol., 14 (2): 185-202.

Christidis G.E., Economou-Eliopolous M., Marcopoulos T. and Laskou M., 1998. An unusual assemblage of high-Ti oxides and ferroan clinochlore along zones of brittle deformation in the Vourinos (Rodiani) Ophiolite Complex, Greece. Can. Mineral., 36 (5): 1327-1338.

Coleman R.G., 1966. New Zealand serpentinites and associated metasomatic rocks. N. Zealand Geol. Surv. Bull., 76(102): 1-102.

Coleman R.G., 1967. Low-temperature reaction zones and Alpine ultramafic rocks of California, Oregon and Washington. U. S. Geol. Surv. Bull., 1247 (1): 1-49.

Coleman R.G., 1977. Ophiolites; ancient oceanic lithosphere? Minerals and rocks. Springer-Verlag, Berlin, 229 pp.

Cortiana G. et al., 1999. Eocene eclogitic imprint in the lower Austroalpine outliers and underlying Zermatt-Saas ophiolites across the Aosta Valley, Western Alps. 4th workshop on Alpine geological studies, Tubingen (Germany). Abstr. Vol., p. 24-25.

Dal Piaz G.B., 1965. Meditazioni geologiche sul "Cristallino Antico" delle Alpi. Atti Rassegne Società Ingegneria e Architettura Torino, 19 (22): 573-576.

Dal Piaz G.V., 1967. Le "granatiti" (rodingiti l.s.) nelle serpentine delle Alpi Occidentali italiane. Mem. Soc. Geol. It., 6 (3): 267-313.

Dal Piaz G.V., 1969. Filoni rodingitici e zone di reazione a bassa temperatura al contatto tettonico tra serpentine e rocce incassanti nelle Alpi Occidentali italiane. Rend. Soc. It. Mineral. Petrol., 25 (2): 263-315.

Dal Piaz G.V., 1988. Revised setting of the Piedmont zone in the northern Aosta Valley, Western Alps. Ofioliti, 13(2-3): 157-162.

Dal Piaz G.V., Di Battistini G., Gosso G. and Venturelli G., 1980. Rodingitic gabbro dykes and rodingitic reaction zones in the upper Valtournanche-Breuil area, Piemonte ophiolite nappe, Italian western Alps. Arch. Sci., 33 (2-3): 161-179.

Dal Piaz G.V. and Ernst W.G., 1978. Areal geology and petrology of eclogites and associated metabasites of the Piemonte ophiolite nappe, Breuil - St. Jacques area, Italian Western Alps. Tectonophysics, 51 (1-2): 99-126.

Dal Piaz G.V., Hunziker J.C. and Martinotti G., 1972. La Zona Sesia-Lanzo e l'evoluzione tettonico-metamorfica delle Alpi Nordoccidentali interne. Mem. Soc. Geol. It., 11 (4): 433-460.

De A., 1972. Petrology of dikes emplaced in the ultramafic rocks of southeastern Québec and origin of the rodingite. Mem. Geol. Soc. Am., 132: 489-501.

Desmons J., Compagnoni R., Frey M. and Gaggero L., 1999. Pre-Alpine metamorphism in the Internal zones of the Western Alps. Schweiz. Mineral. Petrogr. Mitt., 79 (1): 23-40.

Diella V., Ferrario A. and Rossetti P., 1994. The magnetite ore deposits of the southern Aosta Valley; chromitite transformed during an Alpine metamorphic event. Ofioliti, 19 (2A): 247-256.

Dubinska E., Bylina P. and Kozlowski A., 2004a. Garnet from Lower Silesia rodingites: constraints from their chemistry. Mineral. Soc. Poland, Spec. Pap., 24: 135-139.

Dubinska E. et al., 2004b. U-Pb dating of serpentinization: hydrothermal zircon from a metasomatic rodingite shell (Sudetic Ophiolite, SW Poland). Chem. Geol., 203 (3-4): 183-203.

Dubinska E. and Wiewiora A., 1999. Layer silicates from a rodingite and its blackwall from Przemilow (Lower Silesia, Poland): mineralogical record of metasomatic processes during serpentinization and serpentinite recrystallization. Mineral. Petrol., 67 (3-4): 223-237.

Ernst W.G. and Dal Piaz G.V., 1978. Mineral parageneses of eclogitic rocks and related mafic schists of the Piemonte ophiolite nappe, Breuil-St Jacques area, Italian Western Alps. Am. Mineral., 63 (7-8): 621-640.

Evans B.W., Trommsdorff V. and Goles G.G., 1981. Geochemistry of high-grade eclogites and metarodingites from the Central Alps. Contrib. Mineral. Petrol., 76 (3): 301-311.

Evans B.W., Trommsdorff V. and Richter W., 1979. Petrology of an eclogite-metarodingite suite at Cima di Gagnone, Ticino, Switzerland. Am. Mineral., 64 (1-2): 15-31.

Flinn D., 1999. Tressa ness to Colbinstoft. In: D. Stephenson et al. (Editors), Caledonian igneous rocks of Great Britain (17). Geol. Conserv. Rev. Ser..

Fontana E., 2005. Evoluzione oceanica e alpina delle serpentiniti del massiccio del Monte Avic (Valle d'Aosta). Master Thesis, Univ. Studi, Milano, 305 pp.

Fontana E., Panseri,M. and Tartarotti P., 2008. Oceanic relict textures in the mount Avic serpentinites (Western Alps). Ofioliti, 33, this volume.

Fruh-Gree G.L., Plas A. and Lecuyer C., 1996. Petrologic and stable isotope constraints on hydrothermal alteration and serpentinization of the EPR shallow mantle at Hess Deep (Site 895). In: C. Mevel, K.M. Gillis, J.F. Allan and P.S. Meyer (Eds.), Proceed. O.D.P. Sci. Res., LEG147, (147), p. 255-291.

Grange L.I., 1927. On the rodingite of Nelson. Trans. N. Zealand Inst., 58: 160-166.

Grice J.D. and Gasparrini E., 1981. Spertiniite, $Cu(OH)_2$, a new mineral from the Jeffrey Mine, Quebec. Can. Mineral., 19 (2): 337-340.

Hall A. and Ahmed Z., 1984. Rare earth content and origin of rodingites. Chem. Erde, 43 (1): 45-56.

Hatzipanagiotou K. and Tsikouras B., 2001. Rodingite formation from diorite in the Samothraki ophiolite, NE Aegean, Greece. Geol. J., 36 (2): 93-109.

Hatzipanagiotou K., Tsikouras B., Migiros G., Gartzos E. and Serelis K., 2003. Origin of rodingites in ultramafic rocks from Lesvos island (NE Aegean, Greece). Ofioliti, 28 (1): 13-23.

Hey M.H., 1954. A new review of the chlorites. Mineral. Mag., 30 (224): 277-292.

Honnorez J. and Kirst P., 1975. Petrology of rodingites from the equatorial Mid-Atlantic Fracture Zones and their geotectonic significance. Contrib. Mineral. Petrol., 49 (3): 233-257.

Johnson L.E., 1992. Mafic clasts in serpentinite seamounts: petrology and geochemistry of a diverse crustal suite from the outer Mariana forearc. In: P. Fryer, J.A. Pearce and L.B. Stokking (Eds.), Proceed. O. D. P. Sci. Res., LEG125, (125), p. 401-413.

Kelemen B.P. et al., 2003. Ocean Drilling Program: Leg 209 Preliminary Report - Drilling Mantle Peridotite along the Mid-Atlantic Ridge from 14° to 16°N, Ocean Drilling Program, Texas A&M Univ..

Krutow-Mozgawa A., 1988. Metamorphisme eclogitique dans les sediments riches en fer ou magnesium de la couverture des ophiolites piemontaises (mine de Servette, Val d'Aoste). PhD Thesis, Univ. Paris, Paris, 166 pp.

Lagabrielle Y., Bideau D., Cannat M., Karson J.A. and Mével C., 1998. Ultramafic-mafic plutonic rock suites exposed along the Mid-Atlantic Ridge (10°N-30°N). Symmetrical-asymmetrical distribution and implications for seafloor spreading processes, Faulting and magmatism at Mid-Ocean Ridges (160). Geophys. Monograph, Am. Geophys. Union, p. 153-176.

Leblanc M. and Lbouabi M., 1988. Native silver mineralization along a rodingite tectonic contact between serpentinite and quartz diorite (Bou Azzer, Morocco). Econ. Geol., 83 (7): 1379-1391.

Li X.P., Rahn M. and Bucher K., 2004. Metamorphic processes in rodingites of the Zermatt–Saas ophiolites. Intern. Geol. Rev., 46 (1): 28-51.

Li X.P., Rahn M. and Bucher K., 2008. Eclogite facies metarodingites - phase relations in the system SiO_2-Al_2O_3-Fe_2O_2-FeO-MgO-CaO-CO_2-H_2O: an example from the Zermatt-Saas ophiolite. J. Metam. Geol., 26 (3): 347-364.

Li X.P., Zhang L., Wei C., Ai Y. and Chen J.H., 2007. Petrology of rodingite derived from eclogite in western Tianshan, China. J. Metam. Geol., 25 (3): 363-382.

Marthaler M., 1984. Géologie des unités Penniniques entre le Val d'Anniviers et la Val de Tourtemogne (Valais, Swisse). Ecl. Geol. Helv., 7 7(2): 395-448.

Martin S. and Kienast J.R., 1987. The HP-LT manganiferous quartzites of Praborna, Piemonte ophiolite nappe, Italian Western Alps. Schweiz. Mineral. Petrogr. Mitt. 67 (3): 339-360.

Martin S., Rebay G., Kienast J.R. and Mével C., 2008. An eclogitised oceanic palaeo-hydrothermal field from the St. Marcel Valley (Italian Western Alps). Ofioliti, 33 (1): 49-63.

Martin S. and Tartarotti P., 1989. Polyphase HP metamorphism in the ophiolitic glaucophanites of the lower St. Marcel Valley (Aosta, Italy). Ofioliti, 14(3): 135-156.

Martinotti G. and Hunziker J.C., 1984. The Austroalpine system in the Western Alps: a review. Mem. Soc. Geol. I., 29: 43-56.

Michard A., Goffe B., Chopin C. and Henry C., 1996. Did the Western Alps develop through an Oman-type stage? The geotectonic setting of high-pressure metamorphism in two contrasting Tethyan transects. Ecl. Geol. Helv., 89 (1): 43-80.

Mittwede S.K. and Schandl E.S., 1992. Rodingites from the Southern Appalachian Piedmont, South Carolina, USA. Eur. J. Mineral., 4 (1): 7-16.

Mogessie A. and Rammlmair D., 1994. Occurrence of zoned uvarovite-grossular garnet in a rodingite from the Vumba Schist Belt, Botswana, Africa; implications for the origin of rodingites. Mineral. Mag., 58 (3): 375-386.

Nervo R. and Polino R., 1977. Un lembo di cristallino Dent Blanche alla Torre Ponton (Valle d'Aosta). Boll. Soc. Geol. It., 95 (3-4): 647-657.

Nicolas A., Hirn A., Nicolich R., Polino R. and Group E.-C.W., 1990. Lithospheric wedging in the Western Alps inferred from the ECORS-CROP traverse. Geology, 18 (7): 587-590.

Normand C. and Williams-Jones A.E., 2007. Physicochemical conditions and timing of rodingite formation: evidence from rodingite-hosted fluid inclusions in the JM Asbestos mine, Asbestos, Québec. Geochem. Trans., 8 (1): 11.

Novo M., Accotto S., Nervo R. and Pognante U., 1989. Jadeite-quartz bearing metatrondjemites from the Mt. Nero ophiolitic eclogites, Champorcher Valley (Western Alps). Ofioliti, 14 (1/2): 57-62.

O'Hanley D.S., Schandl E.S. and Wicks F.J., 1992. The origin of rodingites from Cassiar, British Columbia, and their use to estimate T and P (H_2O) during serpentinization. Geochim Cosmochim. Acta, 56 (1): 97-108.

Oberhaensli R., 1980. Bestimmungen anhand von Mineralanalysen in Eklogiten und Glaukophaniten der Ophiolite von Zermatt - Translated Title: P-T determinations from mineral analyses of the eclogites and glaucophanites in the Zermatt ophiolite. Schweiz. Mineral. Petrogr. Mitt., 60 (2-3): 215-235.

Oberhaensli R., 1982. The P-T history of some pillow lavas from Zermatt. Ofioliti, 7 (2-3): 431-436.

Ortiz-Hernández L.E., 1999. Petrogénesis de la rodingita del Cretácico Inferior de la Sierra de Guanajuato, México. Rev. Mexic. Ciencias Geol., 16 (2): 147-154.

Panseri M., 2003. Le rodingiti del massiccio serpentinitico del Monte Avic (Valle d'Aosta meridionale): evidenze dell'evoluzione oceanica e alpina della zona ofiolitica piemontese. Master Thesis, Univ. Studi, Milano, 230 pp.

Polino R., Gosso G. and Dal Piaz G.V., 1990. Un modello attualistico sulla genesi delle Alpi. Mem. Soc. Geol. It., 45 (1): 71-75.

Puga E., Nieto J.M., Diaz de Federico A., Bodinier J.L. and Morten L., 1999. Petrology and metamorphic evolution of ultramafic rocks and dolerite dykes of the Betic Ophiolitic Association (Mulhacén Complex, SE Spain): evidence of eo-Alpine subduction following an ocean-floor metasomatic process. Lithos, 49 (1-4): 23-56.

Puschnig A.R., 2002. Metasomatic alterations at mafic-ultramafic contacts in Valmalenco (Rhetic Alps, N-Italy). Schweiz. Mineral. Petrogr. Mitt., 82 (3): 515-536.

Pouchou J.L. and Pichoir F., 1985. PAP phi (rhoZ) procedure for improved quantitative microanalysis. In: J.T. Armstrong (Ed.), Microbeam analysis. San Francisco Press, San Francisco, p. 104-106.

Qaiser M.A., Mansoor Akhter S. and Khan A.H., 1970. Rodingite from Naranji Sar, Dargai ultramafic complex, Malakand, West Pakistan. Mineral. Mag., 37 (290): 735-738.

Reinecke T., 1991. Very high pressure metamorphism and uplift of coesite-bearing metasediments from the Zermatt-Saas Zone, Western Alps. Eur. J. Mineral., 3 (1): 7-17.

Sarp H. and Deferne J., 1978. Le bilan chimique de la rodingitisation et l'origine de l'exces de chaux dans les rodingites. Schweiz. Mineral. Petrogr. Mitt., 58 (3): 315-328.

Sartori M. and Thelin P., 1987. Les schistes illes albitiques de Barneuza (Nappe de Siviez-Mischabel, Valais, Suisse) - Translated Title: Albite-augen schists from Barneuza (Siviriez-Mischabel Nappe), Valais, Switzerland. Schweiz. Mineral. Petrogr. Mitt., 67 (3): 229-256.

Scarrow, J.H. et al., 1999. The Mindyak paleozoic lherzolite ophiolite, Southern Urals: geochemistry and geochronology. Ofioliti, 24 (2): 239-246.

Schandl E., O'Hanley D.S. and Wicks F.J., 1989. Rodingites in serpentinized ultramafic rocks of the Abitibi greenstone belt, Ontario. Can. Mineral., 27 (4): 579-591.

Schandl E.S., O'Hanley D.S., Wicks F.J. and Kyser T.K., 1990. Fluid inclusions in rodingite; a geothermometer for serpentinization. Econ. Geol., 85 (6): 1273-1276.

Siivola J. and Schmid R., 2007. List of mineral abbreviations - Recommendations by the IUGS Subcommission on the Systematics of Metamorphic Rocks. Electronic Source: http://www.bgs.ac.uk/scmr/home.html

Stampfli G.M. and Marchant R.H., 1997. Geodynamic evolution of the Tethyan margins of the Western Alps. In: O.A. Pfiffner, P. Lehner, P. Heitzman, S. Mueller and A. Steck (Eds.), Deep structure of Switzerland-Results from NFP 20. Birkhäuser AG, Basel.

Tartarotti P., 1988. Le ofioliti piemontesi nella media e bassa Valle di St. Marcel (Aosta). PhD Thesis, Univ. Padova, Padova, 120 pp.

Tartarotti P., Benciolini L. and Monopoli B., 1998. Breccie serpentinitiche nel massiccio ultrabasico del Monte Avic (Falda Ofiolitica Piemontese): possibili evidenze di erosione marina. Atti Ticin. Sci. Terra (Serie spec.), 7: 73-86.

Tartarotti P. and Caucia F., 1993. Coexisting cummingtonite - sodic amphibole pair in metaquartzites from the ophiolite's sedimentary cover (St. Marcel Valley, Italian Western Alps); a X-ray structure refinement and petrology study. N. Jahr. Mineral., 165 (3): 223-243.

Tartarotti P. and Martin S., 1991. Ultramafic rocks in the Mount Avic eclogitic ophiolites, Italian Western Alps. Terra Abstr.s, 3 (1): 96.

Tartarotti P., Martin S. and Polino R., 1986. Geological data about the ophiolitic sequences in the St. Marcel Valley (Aosta Valley). Ofioliti, 11 (3): 343-346.

Tribuzio R., Tiepolo M. and Vannucci R., 2000. Evolution of gabbroic rocks of the Northern Apennine ophiolites (Italy): comparison with the lower oceanic crustfrom modern, Ophiolites and oceanic crust: new insights from field studies and the Ocean Drilling Program. Geol. Soc. Am. Spec. Pap., 349: 129-138.

Van der Klauw S.N.G.C., Reinecke T. and Stockhert B., 1997. Exhumation of ultrahigh-pressure metamorphic oceanic crust from Lago di Cignana, Piemontese zone, western Alps: the structural record in metabasites. Lithos, 41 (1-3): 79-102.

Zharikov V.A., Pertsev N.N., Rusinov V.L., Callegari E. and Fettes D.J., 2007. Metasomatism and metasomatic rocks - Recommendations by the IUGS Subcommission on the Systematics of Metamorphic Rocks. Electronic Source: http://www.bgs.ac.uk/scmr/home.html

Received, April 14, 2008
Accepted, November 21, 2008